Technische Universität Chemnitz

Sonderforschungsbereich 393

Numerische Simulation auf massiv parallelen Rechnern

Emmanuel Creusé, Gerd Kunert, Serge Nicaise

A posteriori error estimation for the Stokes problem: Anisotropic and isotropic discretizations

Abstract

The paper presents *a posteriori* error estimators for the stationary Stokes problem. We consider *anisotropic* finite element discretizations (i.e. elements with very large aspect ratio) where conventional, isotropic error estimators fail.

Our analysis covers two- and three-dimensional domains, conforming and nonconforming discretizations as well as different elements. This large variety of settings requires different approaches and results in different estimators. Furthermore many examples of finite element pairs that are covered by the analysis are presented.

Lower and upper error bounds form the main result with minimal assumptions on the elements. The lower error bound is uniform with respect to the mesh anisotropy with the exception of nonconforming 3D discretizations made of pentahedra or hexahedra. The upper error bound depends on a proper alignment of the anisotropy of the mesh which is a common feature of anisotropic error estimation.

In the special case of isotropic meshes, the results simplify, and upper and lower error bounds hold unconditionally. Some of the corresponding results seem to be novel (in particular for 3D domains), and cover element pairs of practical importance.

The numerical experiments confirm the theoretical predictions and show the usefulness of the anisotropic error estimators.

Keywords: error estimator, anisotropic solution, stretched elements, Stokes problem
AMS: 65N15, 65N30, 76D07

Contents

1   Introduction

In this paper we consider the stationary Stokes problem with Dirichlet boundary conditions: given a (vector) function $\underline{f}$ find a vector function $\underline{u}$, the velocity of the fluid and a (scalar) function p, the pressure, satisfying

$$\left.\begin{array}{rcll} -\Delta \underline{u} + \nabla p & = & \underline{f} & \text{in } \Omega \\ \text{div } \underline{u} & = & 0 & \text{in } \Omega \\ \underline{u} & = & 0 & \text{on } \partial\Omega. \end{array}\right\} \tag{1}$$

In certain situations the solution has strong directional features, for example edge singularities. Such a so-called *anisotropic solution* occurs e.g. for concave edges in three dimensional domains, cf. [ANS01b]. Then it is natural to reflect the anisotropy in a suitable finite element discretization by using so-called *anisotropic elements*. These are stretched elements where the aspect ratio can be very large, i.e. the ratio of the radii of the circumscribed and inscribed sphere is (potentially) unbounded. Although this is in contrast with the conventional, isotropic theory, the use of anisotropic discretizations allows to achieve the same accuracy with (much) less degrees of freedom. For more details see [Ape99] and the citations therein.

Here we are concerned with *a posteriori* error estimators which are vitally important for adaptive algorithms and quality control. Particular emphasis is given to the Stokes problem in 3D domains since anisotropic solutions arise there generically. Furthermore we also treat nonconforming discretizations because they are frequently applied and (comparatively) simple to implement.

There has been much research for a posteriori error estimators for isotropic discretizations of the Stokes problem (mainly for 2D domains), cf. [Ver89, BW90, DDP95, AO97, KS00, CF01] to name but a few. On anisotropic meshes, however, these isotropic estimators usually fail since the lower and upper error bound differ by a factor which is (at most) proportional to the aspect ratio of the anisotropic elements. This potentially unbounded factor renders the isotropic, conventional estimators useless. Hence in the last decade there has been increasing research to find adapted estimators for anisotropic meshes, cf. [Sie96, Kun99, Kun00, Kun01, FPZ01, DGP99, Ran01]. It turns out that the *upper error bound* is the crucial issue which involves a proper alignment of the anisotropic mesh, see e.g. [Kun00]. Thus we may examine the existing approaches to derive upper error bounds for the Stokes problem on *isotropic* meshes. One encounters just a few techniques (which can partially overlap):

- the residual error estimator method for conforming approximations based on the continuous inf-sup condition [Ver89, KS00],
- the residual error estimator method for nonconforming approximation based on the continuous inf-sup condition (applied to the pressure error alone) and on a Helmholtz like decomposition of the error [DDP95, CF01][1],

---

[1]The paper [Ver91] has a similar aim but the consistency error (which is related to tangential gradient jumps) is omitted although it is not of higher order in general.

- the hierarchical basis method based on a saturation assumption [Ban98, Ran01],
- the local residual method which requires the solution of local Stokes problems [Ver89, BW90, KS00], or of local Poisson problem [AO97, JL00],
- error estimation by duality arguments [Joh98, Bec00, Bur01].

Our goal here is to extend the residual error estimator methods to anisotropic meshes in 2D and 3D domains and to both conforming and nonconforming discretizations. We endeavour to identify minimal assumptions on the elements in order to obtain an equivalence between the error norm and the residual error. This approach allows to make an unified analysis and to extend former results obtained for particular elements on isotropic meshes to a large class of elements on isotropic and anisotropic meshes.

The paper is organized as follows. Section 2 introduces the problem and some notation. The discretization (as a mixed formulation) and general conditions on the mesh and the element pairs are given in Section 3. Section 4 is devoted to analytical tools. The specific anisotropic interpolation estimates are particularly important. It turns out that an anisotropic mesh should be well aligned with the anisotropic solution. This demand seems to be an inherent feature of anisotropic discretizations and error estimates. In Section 5 we present several examples of element pairs that are covered by our analysis. To our knowledge, some of these elements are new. The actual error bounds are given in Section 6. For the upper error bound, we additionally distinguish between conforming and nonconforming discretization. While all these considerations are made for anisotropic meshes, we simplify the results for the case of an isotropic discretization in Section 6.4. There several restrictions for anisotropic elements disappear. The numerical experiments of Section 7 confirm our theoretical predictions.

Our exposition treats the two dimensional case ($d = 2$) as well as the three dimensional case ($d = 3$). Where both cases require a different treatment, we present the 2D case and list the modifications for the 3D case.

2   Preliminaries and notation

Let us fix a bounded domain Ω of $\mathbb{R}^d$, $d = 2$ or 3, with a Lipschitz boundary, and consider the Stokes problem (1). To obtain the corresponding weak formulation, introduce the spaces

$$
\begin{aligned}
V = [H_0^1(\Omega)]^d &:= \{\underline{v} \in [H^1(\Omega)]^d : \underline{v} = \underline{0} \text{ on } \partial\Omega\}, \\
Q = L_0^2(\Omega) &:= \{q \in L^2(\Omega) : \int_\Omega q = 0\},
\end{aligned}
$$

and the bilinear forms

$$
a(\underline{u}, \underline{v}) := \int_\Omega \nabla\underline{u} : \nabla\underline{v}, \qquad b(\underline{v}, q) := -\int_\Omega q\,\mathrm{div}\,\underline{v},
$$

where here and below $\nabla \underline{u}$ means the matrix $(\partial_j u_i)_{1 \leq i,j \leq d}$ (i being the index of row and j the index of column). We use the standard notation for the contraction of two matrices $\underline{\underline{A}}$ and $\underline{\underline{B}}$, i.e.,

$$\underline{\underline{A}} : \underline{\underline{B}} := \sum_{i,j=1}^{d} A_{ij} B_{ij}.$$

The norm and seminorm of the standard Sobolev space $H^1(D)$ is denoted by $\| \cdot \|_{H^1(D)}$ and $| \cdot |_{H^1(D)}$, respectively. The $L^2(D)$ norm is denoted by $\| \cdot \|_D$. In the case $D = \Omega$, we will drop the index Ω.

According to Theorem I.5.1 of [GR86], for $\underline{f} \in L^2(\Omega)^d$, there exists a unique solution $(\underline{u}, p) \in V \times Q$ of

$$\left. \begin{array}{rcll} a(\underline{u}, \underline{v}) + b(\underline{v}, p) & = & (\underline{f}, \underline{v}) & \forall v \in V, \\ b(\underline{u}, q) & = & 0 & \forall q \in Q, \end{array} \right\} \tag{2}$$

where $(\cdot, \cdot)$ means the inner product in $[L^2(\Omega)]^d$ or in $L^2(\Omega)$ according to the context.

We end this section with some notation and some partial integrations that will be used in the remainder of the paper. The notation $\underline{u}$ (resp. $\underline{A}$) means that the quantity u (resp. A) is a vector (resp. a matrix).

In 2D, the $\underline{\mathrm{curl}}$ of a scalar function w is given as usual by $\underline{\mathrm{curl}}\, w := (-\partial_2 w, \partial_1 w)^\top$. For a vector function $\underline{w}$, we define $\underline{\underline{\mathrm{curl}}}\, \underline{w}$ rowwise:

$$\underline{\underline{\mathrm{curl}}}\, \underline{w} := \left[\begin{array}{c} (\underline{\mathrm{curl}}\, w_1)^\top \\ (\underline{\mathrm{curl}}\, w_2)^\top \end{array} \right] = \left[\begin{array}{cc} -\partial_2 w_1 & \partial_1 w_1 \\ -\partial_2 w_2 & \partial_1 w_2 \end{array} \right].$$

In 3D, the $\underline{\mathrm{curl}}$ of a vector function $\underline{w}$ is given as usual by $\underline{\mathrm{curl}}\, \underline{w} := \nabla \times \underline{w}$. For a matrix function $\underline{\underline{w}}$ we define $\underline{\underline{\mathrm{curl}}}\, \underline{\underline{w}}$ as well as $\underline{\underline{Matrix}} \times \underline{n}$ rowwise:

$$\underline{\underline{\mathrm{curl}}}\, \underline{\underline{w}} := \left[\begin{array}{c} (\underline{\mathrm{curl}}\, \underline{row}_1)^\top \\ (\underline{\mathrm{curl}}\, \underline{row}_2)^\top \\ (\underline{\mathrm{curl}}\, \underline{row}_3)^\top \end{array} \right] \qquad \underline{\underline{Matrix}} \times \underline{n} := \left[\begin{array}{c} (\underline{row}_1 \times \underline{n})^\top \\ (\underline{row}_2 \times \underline{n})^\top \\ (\underline{row}_3 \times \underline{n})^\top \end{array} \right].$$

Let us recall standard Green's formula in d spatial dimensions: for $\omega \subset \mathbb{R}^d$ with a Lipschitz boundary, for any $q \in H^1(\omega); \underline{v} \in [H^2(\omega)]^d, \underline{w} \in [H^1(\omega)]^d$, we have

$$\int_\omega \nabla \underline{v} : \nabla \underline{w} + \Delta \underline{v} \cdot \underline{w} = \int_{\partial \omega} \nabla \underline{v}\, \underline{n} \cdot \underline{w} \tag{3}$$

$$\int_\omega q\mathrm{I} : \nabla \underline{w} + \nabla q \cdot \underline{w} = \int_{\partial \omega} q\mathrm{I}\underline{n} \cdot \underline{w}, \tag{4}$$

where $\underline{n}$ means the outer normal vector along $\partial \omega$.

By (4), in 2D we then have for all $\underline{v}, \underline{w} \in [H^1(\omega)]^2$:

$$\int_\omega \nabla \underline{v} : \underline{\underline{\mathrm{curl}}}\, \underline{w} = \int_{\partial \omega} (\nabla \underline{v}\, \underline{t}) \cdot \underline{w} = -\int_{\partial \omega} \underline{v} \cdot (\nabla \underline{w}\, \underline{t}) = \int_{\partial \omega} \underline{v} \cdot (\underline{\underline{\mathrm{curl}}}\, \underline{w}\, \underline{n}), \tag{5}$$

where $\underline{t}$ is the (positively oriented) unit tangent vector along $\partial\omega$.

Similarly in 3D, for any $\underline{v} \in [H^1(\omega)]^3, \underline{\underline{w}} \in [H^1(\omega)]^{3\times3}$ it holds

$$\int_\omega \nabla\underline{v} : \underline{\mathrm{curl}}\,\underline{\underline{w}} \;=\; \int_{\partial\omega} (\nabla\underline{v}\times\underline{n}) : \underline{\underline{w}} \;=\; \int_{\partial\omega} \underline{v}\cdot(\underline{\mathrm{curl}}\,\underline{\underline{w}}\,\underline{n}). \tag{6}$$

Finally, let $\mathbb{P}^k$ and $\mathbb{Q}^k$ be the space of polynomials of total and partial degree not larger than k, respectively. In order to avoid excessive use of constants, the abbreviations $x \lesssim y$ and $x \sim y$ stand for $x \leq cy$ and $c_1 x \leq y \leq c_2 x$, respectively, with positive constants independent of x, y or $\mathcal{T}$.

3   Discretization

3.1   Discretization of the domain Ω

The domain Ω is discretized by a conforming mesh $\mathcal{T}$, cf. [Cia78]. In 2D, all elements are either triangles or rectangles. In 3D the mesh consists either of tetrahedra, of rectangular hexahedra, or of rectangular pentahedra (i.e. prisms where the triangular faces are orthogonal to the rectangular faces), cf. also the figures of Section 3.3.

Elements will be denoted by T, T_i or T', its edges (in 2D) or faces (in 3D) are denoted by E. The set of all (interior and boundary) edges (2D) or faces (3D) of the triangulation will be denoted by $\mathcal{E}$. In 3D we further use the set of all rectangular faces of the triangulation that we shall denote by $\mathcal{E}_\square$. Let $\underline{x}$ denote a nodal point, and let $\mathcal{N}_\Omega$ be the set of internal nodes of the mesh. The measure of an element or edge/face is denoted by $|T| := \mathrm{meas}_d(T)$ and $|E| := \mathrm{meas}_{d-1}(E)$, respectively.

For an edge E of a 2D element T introduce the *outer normal vector* by $\underline{n} = (n_x, n_y)^\top$. Similarly, for a face E of a 3D element T set $\underline{n} = (n_x, n_y, n_z)^\top$. Furthermore, for each face E we fix one of the two normal vectors and denote it by $\underline{n}_E$. In the 2D case introduce additionally the *tangent vector* $\underline{t} = \underline{n}^\perp := (-n_y, n_x)^\top$ such that it is oriented positively (with respect to T). Similarly set $\underline{t}_E := \underline{n}_E^\perp$.

The *jump* of some (scalar or vector valued) function v across a face E at a point $\underline{y} \in E$ is then defined as

$$[\![v(\underline{y})]\!]_E := \begin{cases} \displaystyle\lim_{\alpha\to+0} v(\underline{y}+\alpha\underline{n}_E) - v(\underline{y}-\alpha\underline{n}_E) & \text{for an interior face } E, \\[2mm] v(y) & \text{for a boundary face } E. \end{cases}$$

Note that the sign of $[\![v]\!]_E$ depends on the orientation of $\underline{n}_E$. However, terms such as a gradient jump $[\![\nabla v\,\underline{n}_E]\!]_E$ are independent of this orientation.

Furthermore one requires local subdomains (also known as patches). As usual, let ω_T be the union of all elements having a common face with T. Similarly let ω_E be the union of both elements having E as face (with appropriate modifications for a boundary face). By $\omega_{\underline{x}}$ we denote the union of all elements having $\underline{x}$ as node.

If we have $\underline{v} \in [H^1(T)]^d$ for all T in $\mathcal{T}$, then we can define a *broken gradient norm* on a subset ω of Ω by :

$$\|\nabla_{\mathcal{T}} \, \underline{v}\|_\omega^2 := \sum_{T \subset \omega} \|\nabla \underline{v}\|_T^2.$$

Later on we specify additional, mild mesh assumptions that are partially due to the anisotropic discretization.

3.2   Discrete mixed formulation

We assume a given velocity (resp. pressure) approximation space V_{veloc} (resp. Q_{pre}) made of polynomials on each element T of the triangulation $\mathcal{T}$ and such that $Q_{\text{pre}} \subset Q$ (but not necessarily $V_{\text{veloc}} \subset V$). A precise description of the properties that these approximation spaces V_{veloc} and Q_{pre} have to satisfy is given in Section 3.4. Moreover many examples of suitable spaces are presented in Section 5.

Since the velocity approximation space V_{veloc} may not be included in the velocity space V, we define the approximate solution by using the weaker bilinear forms $a_h(.,.)$ and $b_h(.,.)$:

$$a_h(\underline{u}, \underline{v}) \quad := \quad \sum_{T \in \mathcal{T}} \int_T \nabla \underline{u} : \nabla \underline{v}, \qquad \forall \underline{u}, \underline{v} \in V_{\text{veloc}}, \tag{7}$$

$$b_h(\underline{u}, q) \quad := \quad -\sum_{T \in \mathcal{T}} \int_T q \operatorname{div} \underline{u}, \qquad \forall \underline{u} \in V_{\text{veloc}}, q \in Q_{\text{pre}}. \tag{8}$$

The mixed finite element formulation reads now: Find $\underline{u}_h \in V_{\text{veloc}}, p_h \in Q_{\text{pre}}$, such that

$$\left. \begin{array}{rcll} a_h(\underline{u}_h, \underline{v}_h) + b_h(\underline{v}_h, p_h) & = & (\underline{f}, \underline{v}_h) & \forall \underline{v}_h \in V_{\text{veloc}}, \\ b_h(\underline{u}_h, q_h) & = & 0 & \forall q_h \in Q_{\text{pre}}. \end{array} \right\} \tag{9}$$

The space V_{veloc} is equipped with the seminorm $\|\underline{v}\|_{1,h} := \|\nabla_{\mathcal{T}} \underline{v}\|_\Omega = a_h^{1/2}(\underline{v}, \underline{v})$.

For $\underline{v} \in [H_0^1(\Omega)]^d \cap V_{\text{veloc}}$ we can subtract (2) and (7) to obtain the 'Galerkin orthogonality' relation

$$\int_\Omega \nabla_{\mathcal{T}} \, \underline{e} : \nabla \underline{v} - \int_\Omega \varepsilon \operatorname{div} \underline{v} = 0 \qquad \forall \, \underline{v} \in [H_0^1(\Omega)]^d \cap V_{\text{veloc}}, \tag{10}$$
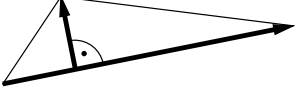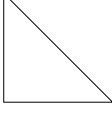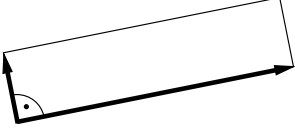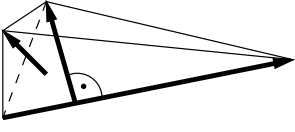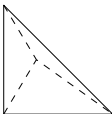
where here and below, the error in the velocity and in the pressure are respectively defined by

$$\underline{e} := \underline{u} - \underline{u}_h, \qquad \varepsilon := p - p_h.$$

3.3   Finite element domains T and reference domains

In our exposition T can be a triangle or rectangle (2D case), or a tetrahedron, a (rectangular) hexahedron, or a prismatic pentahedron (3D case).

Parts of the analysis require *reference elements* $\bar{T}$ that can be obtained from the actual element T via some affine linear transformation. The table below lists the reference elements for each case. Furthermore for an element T we define 2 or 3 *anisotropy vectors* $\underline{p}_{i,T}, i = 1 \ldots d$, that reflect the main anisotropy directions of that element. These anisotropy vectors are defined and visualized in the table below as well.

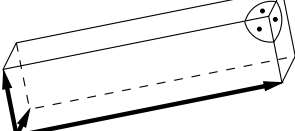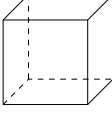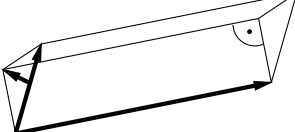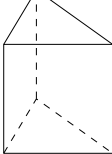| Element T	Reference element $\bar{T}$	Anisotropy vectors $\underline{p}_{i,T}$
Triangle	$0 \le \bar{x}, \bar{y}$ $\bar{x} + \bar{y} \le 1$	$\underline{p}_{1,T}$ longest edge $\underline{p}_{2,T}$ height vector
Rectangle	$0 \le \bar{x}, \bar{y} \le 1$	$\underline{p}_{1,T}$ longest edge $\underline{p}_{2,T}$ height vector
Tetrahedron	$0 \le \bar{x}, \bar{y}, \bar{z}$ $\bar{x} + \bar{y} + \bar{z} \le 1$	$\underline{p}_{1,T}$ longest edge $\underline{p}_{2,T}$ height in largest face that contains $\underline{p}_{1,T}$ $\underline{p}_{3,T}$ remaining height
Hexahedron	$0 \le \bar{x}, \bar{y}, \bar{z} \le 1$	$\underline{p}_{1,T}$ longest edge $\underline{p}_{2,T}$ height in largest face that contains $\underline{p}_{1,T}$ $\underline{p}_{3,T}$ remaining height
Pentahedron (Prism)	$0 \le \bar{x}, \bar{y}, \bar{z} \le 1$ $\bar{x} + \bar{y} \le 1$	longest edge in triangle; height in triangle; height over triangle (see figure)

The anisotropy vectors $\underline{p}_{i,T}$ are enumerated such that their lengths are decreasing, i.e. $|\underline{p}_{1,T}| \ge |\underline{p}_{2,T}| \ge |\underline{p}_{3,T}|$ in the 3D case, and analogously in 2D. The *anisotropic lengths* of an element T are now defined by

$$h_{i,T} := |\underline{p}_{i,T}|$$

which implies $h_{1,T} \ge h_{2,T} \ge h_{3,T}$ in 3D. The smallest of these lengths is particularly important; thus we introduce

$$h_{min,T} := h_{d,T} \equiv \min_{i=1\ldots d} h_{i,T}.$$

Finally the anisotropy vectors $\underline{p}_{i,T}$ are arranged columnwise to define a matrix

$$\left. \begin{array}{rcll} \underline{\underline{C}}_T & := & [\underline{p}_{1,T}, \underline{p}_{2,T}] \in \mathbb{R}^{2\times 2} & \text{in 2D} \\ \underline{\underline{C}}_T & := & [\underline{p}_{1,T}, \underline{p}_{2,T}, \underline{p}_{3,T}] \in \mathbb{R}^{3\times 3} & \text{in 3D.} \end{array} \right\} \tag{11}$$

Note that $\underline{\underline{C}}_T$ is orthogonal since the anisotropy vectors $\underline{p}_{i,T}$ are orthogonal too, and

$$\underline{\underline{C}}_T^\top \underline{\underline{C}}_T = \mathrm{diag}\{h_{1,T}^2, \ldots, h_{d,T}^2\}.$$

Furthermore introduce the *height* $h_{E,T}$ over an edge/face E of an element T by

$$h_{E,T} := \frac{|T|}{|E|} \cdot \begin{cases} 1 & T \text{ is rectangle or hexahedron} \\ d & T \text{ is triangle or tetrahedron} \\ 1 & \text{for triangular face } E \text{ of pentahedron } T \\ 2 & \text{for rectangular face } E \text{ of pentahedron } T. \end{cases}$$

In 3D, we further need the minimal size $\varrho(E)$ of a rectangular face $E \in \mathcal{E}_\square$, i.e., $\varrho(E)$ is the smallest of the lengths of the edges of E.

3.4 Requirements on the mesh and the elements

Mesh assumptions:

The mesh has to satisfy some mild assumptions.

- The mesh is conforming in the standard sense of [Cia78].
- A node $\underline{x}_j$ of the mesh is contained only in a bounded number of elements.
- The size of neighbouring elements does not change rapidly, i.e.

$$h_{i,T_1} \sim h_{i,T_2} \qquad \forall i = 1 \ldots d, \forall T_1 \cap T_2 \neq \emptyset.$$

Sometimes it is more convenient to have *face related* data instead of *element related* data. Hence for an interior face $E = T_1 \cap T_2$ we introduce

$$h_{min,E} := \frac{h_{min,T_1} + h_{min,T_2}}{2} \qquad \text{and} \qquad h_E := \frac{h_{E,T_1} + h_{E,T_2}}{2}.$$

For boundary faces $E \subset \partial T$ simply set $h_{min,E} := h_{min,T}$, $h_E := h_{E,T}$. The last assumption from above readily implies

$$h_E \sim h_{E,T_1} \sim h_{E,T_2} \qquad \text{and} \qquad h_{min,E} \sim h_{min,T_1} \sim h_{min,T_2}.$$

Note that in 3D and for a face $E \in \mathcal{E}_\square$, $h_{min,E}$ has no direct relation with $\varrho(E)$.

General Assumptions:

In our analysis, a Clément type interpolation operator $\mathrm{I}_{\mathrm{Cl}}^0$ plays a vital role. Although the precise definition will be postponed until Section 4.2, we briefly describe the image space of this operator. Roughly speaking, its functions are continuous and piecewise linear for triangles and tetrahedra T, and piecewise bi-/trilinear for rectangles/hexahedra. For a detailed description (and the definition for pentahedra) see Section 4.2. From now on, we use the notation

$$V_{\mathrm{Cl}}^0 := [\mathrm{Im}(\mathrm{I}_{\mathrm{Cl}}^0)]^d$$

for the Clément interpolation space.

The general conditions are now as follows.

(G1) The velocity space V_{veloc} is large enough such that it contains the Clément interpolation space, i.e. $[\text{Im}(\text{I}_{\text{Cl}}^0)]^d \equiv V_{\text{Cl}}^0 \subset [H_0^1(\Omega)]^d \cap V_{\text{veloc}}$.

(G2) In order to obtain robust discrete solutions, the element pairs have to be stable (i.e. the discrete inf-sup condition is satisfied). Note that this condition is not necessary to prove error bounds, but in particular it guarantees existence and uniqueness of the discrete solution of (9).

We remark here that an accurate nonconforming discretizations also requires a small *consistency error*. For some of the example element pairs below, this has been proven already, cf. [ANS01b] for example. Nevertheless this question is not of primary interest in our work.

Crouzeix-Raviart property for nonconforming approximation:

For nonconforming approximation we require the "Crouzeix-Raviart" property:

(CR) $\quad \displaystyle\int_E [\![\underline{u}_h]\!]_E = \underline{0} \qquad \forall \underline{u}_h \in V_{\text{veloc}}, \ E \in \mathcal{E}.$
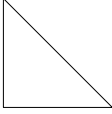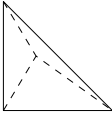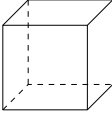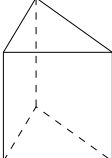
Note that for boundary faces E this simplifies to $\int_E \underline{u}_h = \underline{0}$.

4   Analytical tools

4.1   Bubble functions, extension operator, inverse inequalities

For the analysis we require bubble functions and extension operators that satisfy certain properties. We start with the reference element $\bar{T}$ and define an *element bubble function* $b_{\bar{T}} \in C(\bar{T})$. We also require an *edge bubble function* $b_{\bar{E},\bar{T}} \in C(\bar{T})$ for an edge $\bar{E} \subset \partial\bar{T}$ (2D case), and a *face bubble function* $b_{\bar{E},\bar{T}} \in C(\bar{T})$ for a face $\bar{E} \subset \partial\bar{T}$ (3D case). Without loss of generality assume that $\bar{E}$ is on the $\bar{x}$ axis (2D case) or in the $\bar{x}\bar{y}$ plane (tetrahedral and hexahedral case). For the pentahedral case, the triangular face $\bar{E}_\triangle$ is also in the $\bar{x}\bar{y}$ plane but the rectangular face $\bar{E}_\square$ is in the $\bar{x}\bar{z}$ plane.

Furthermore an *extension operator* $\text{F}_{\text{ext}} : C(\bar{E}) \to C(\bar{T})$ will be necessary that acts on some function $v_{\bar{E}} \in C(\bar{E})$. The table below gives the definitions in each case. For vector valued functions apply the extension operator componentwise.

Ref. element $\bar{T}$	Bubble functions	Extension operator
	$b_{\bar{T}} := 3^3 \bar{x}\bar{y}(1-\bar{x}-\bar{y})$ $b_{\bar{E},\bar{T}} := 2^2 \bar{x}(1-\bar{x}-\bar{y})$	$\mathrm{F}_{\mathrm{ext}}(v_{\bar{E}})(\bar{x},\bar{y}) := v_{\bar{E}}(\bar{x})$
	$b_{\bar{T}} := 2^4 \bar{x}(1-\bar{x})\bar{y}(1-\bar{y})$ $b_{\bar{E},\bar{T}} := 2^2 \bar{x}(1-\bar{x})(1-\bar{y})$	$\mathrm{F}_{\mathrm{ext}}(v_{\bar{E}})(\bar{x},\bar{y}) := v_{\bar{E}}(\bar{x})$
	$b_{\bar{T}} := 4^4 \bar{x}\bar{y}\bar{z}(1-\bar{x}-\bar{y}-\bar{z})$ $b_{\bar{E},\bar{T}} := 3^3 \bar{x}\bar{y}(1-\bar{x}-\bar{y}-\bar{z})$	$\mathrm{F}_{\mathrm{ext}}(v_{\bar{E}})(\bar{x},\bar{y},\bar{z}) := v_{\bar{E}}(\bar{x},\bar{y})$
	$b_{\bar{T}} := 2^6 \bar{x}(1-\bar{x})\bar{y}(1-\bar{y})\bar{z}(1-\bar{z})$ $b_{\bar{E},\bar{T}} := 2^4 \bar{x}(1-\bar{x})\bar{y}(1-\bar{y})(1-\bar{z})$	$\mathrm{F}_{\mathrm{ext}}(v_{\bar{E}})(\bar{x},\bar{y},\bar{z}) := v_{\bar{E}}(\bar{x},\bar{y})$
	$b_{\bar{T}} := 3^3 2^2 \bar{x}\bar{y}(1-\bar{x}-\bar{y})\bar{z}(1-\bar{z})$ $b_{\bar{E},\bar{T},\triangle} := 3^3 \bar{x}\bar{y}(1-\bar{x}-\bar{y})(1-\bar{z})$ $b_{\bar{E},\bar{T},\square} := 2^4 \bar{x}(1-\bar{x}-\bar{y})\bar{z}(1-\bar{z})$	$\mathrm{F}_{\mathrm{ext}}(v_{\bar{E}_{\triangle}})(\bar{x},\bar{y},\bar{z}) := v_{\bar{E}_{\triangle}}(\bar{x},\bar{y})$ $\mathrm{F}_{\mathrm{ext}}(v_{\bar{E}_{\square}})(\bar{x},\bar{y},\bar{z}) := v_{\bar{E}_{\square}}(\bar{x},\bar{z})$

The element bubble function b_T for the actual element T is obtained simply by the corresponding affine linear transformation. Similarly the edge/face bubble function $b_{E,T}$ is defined. Later on an edge/face bubble function b_E is needed on the domain $\omega_E = T_1 \cup T_2$. This is achieved by an elementwise definition, i.e.

$$b_E|_{T_i} := b_{E,T_i}, \qquad i = 1, 2.$$

Analogously the extension operator is defined for functions $v_E \in C(E)$. By the same elementwise definition obtain then $\mathrm{F}_{\mathrm{ext}}(v_E) \in C(\omega_E)$. With these definitions one easily checks

$$b_T = 0 \text{ on } \partial T, \qquad b_E = 0 \text{ on } \partial\omega_E, \qquad \|b_T\|_{\infty,T} = \|b_E\|_{\infty,\omega_E} = 1.$$

Next, one requires so-called *inverse inequalities*. They can only be expected to hold in some finite dimensional space. The choice $\mathbb{P}^k$ covers all relevant cases of our analysis.

Lemma 4.1 (Inverse inequalities) *Let $E \subset \partial T$ be an edge/face of an element T. Consider $\underline{v}_T \in \mathbb{P}^{k_0}(T)$ and $\underline{v}_E \in \mathbb{P}^{k_1}(E)$. Then the following equivalences/inequalities hold. The inequality constants depend on the polynomial degree k_0 or k_1 but not on T, E or $\underline{v}_T$, $\underline{v}_E$.*

$$\|\underline{v}_T b_T^{1/2}\|_T \quad \sim \quad \|\underline{v}_T\|_T \tag{12}$$

$$\|\nabla(\underline{v}_T b_T)\|_T \quad \lesssim \quad h_{min,T}^{-1}\|\underline{v}_T\|_T \tag{13}$$

$$\|\underline{v}_E b_E^{1/2}\|_E \quad \sim \quad \|\underline{v}_E\|_E \tag{14}$$

$$\|\mathrm{F}_{\mathrm{ext}}(\underline{v}_E)b_E\|_T \quad \lesssim \quad h_{E,T}^{1/2}\|\underline{v}_E\|_E \tag{15}$$

$$\|\nabla(\mathrm{F}_{\mathrm{ext}}(\underline{v}_E)b_E)\|_T \;\lesssim\; h_{E,T}^{1/2}h_{min,T}^{-1}\|\underline{v}_E\|_E \tag{16}$$

$$\|\underline{\mathrm{curl}}\;(\mathrm{F}_{\mathrm{ext}}(\underline{v}_E)b_E)\|_T \;\lesssim\; h_{E,T}^{1/2}h_{min,T}^{-1}\|\underline{v}_E\|_E \qquad (only\ in\ 3D.) \tag{17}$$

Proof: The proof employs scaling techniques but now with transformations that are specifically tailored for anisotropic elements. For the rectangular and hexahedral case, details are given in [Sie96, Lemma 5.1]. The more sophisticated triangular and tetrahedral case is treated in [Kun99, Section 2.3.3] (for $k_0 = 0$ and $k_1 = 1$). The ideas presented there can be extended to cover the remaining cases as well. ∎

4.2   Clément interpolation

For the analysis we require some interpolation operator that maps a function from $H_0^1(\Omega)$ to some continuous, piecewise polynomial function V_{Cl}^0. Hence Lagrange interpolation is unsuitable, but Clément like interpolation techniques have proven to be useful. The image space V_{Cl}^0 will be given by means of its basis functions. To this end denote by F_T temporarily that affine linear transformation that maps the reference element $\bar{T}$ onto the actual element T. For simplicity we describe the interpolation for scalar functions; for vector valued functions the interpolation acts componentwise.

The basis function φ_j associated with a node $\underline{x}_j$ is now uniquely determined by the condition

$$\varphi_j(\underline{x}_i) = \delta_i^j \qquad \forall \underline{x}_i \in \mathcal{N}_\Omega,$$

and by the polynomial space of $\varphi_j|T$:

Finite element domain T	Local space $\mathcal{P}_T$ of $\varphi_j|_T \circ F_T$
Triangle, Tetrahedron	$\mathbb{P}^1(\bar{T})$
Rectangle, Hexahedron	$\mathbb{Q}^1(\bar{T})$
Pentahedron	$\mathrm{span}\{1, \bar{x}, \bar{y}, \bar{z}, \bar{x}\bar{z}, \bar{y}\bar{z}\}$

Then V_{Cl}^0 is defined as the space spanned by the functions φ_j, for all interior nodes $x_j \in \mathcal{N}_\Omega$. Equivalently, it can be expressed as

$$V_{\mathrm{Cl}}^0 := \{v_h \in C(\Omega) : v_h = 0 \text{ on } \partial\Omega,\ v_h|_T \circ F_T \in \mathcal{P}_T\} \subset H_0^1(\Omega), \tag{18}$$

with $F_T, \mathcal{P}_T$ as above. With the exception of the pentahedron, the space V_{Cl}^0 consists of the usual continuous and piecewise linear, bilinear or trilinear functions, respectively.

Next, the Clément interpolation operator will be defined via the basis functions $\varphi_j \in V_{\mathrm{Cl}}^0$.

Definition 4.2 (Clément interpolation operator) *Consider an interior node* $\underline{x}_j \in \mathcal{N}_\Omega$ *and the patch* $\omega_{\underline{x}_j} \equiv supp(\varphi_j)$, *cf. Section 3.1. Define the* local L^2 *projection operator* $P_j : L^2(\omega_{\underline{x}_j}) \to \mathbb{P}^0(\omega_{\underline{x}_j})$ *by*

$$\int_{\omega_{\underline{x}_j}} (v - P_j v)w = 0 \qquad \forall w \in \mathbb{P}^0(\omega_{\underline{x}_j}).$$

For vector valued functions $\underline{v} \in [L^2(\omega_{\underline{x}_j})]^d$ define the projection componentwise.

Then define the Clément interpolation operator $\mathrm{I}_{\mathrm{Cl}}^0 : H_0^1(\Omega) \to V_{\mathrm{Cl}}^0 \subset H_0^1(\Omega)$ *by*

$$\mathrm{I}_{\mathrm{Cl}}^0 v := \sum_{\underline{x}_j \in \mathcal{N}_\Omega} P_j(v)(\underline{x}_j) \, \varphi_j.$$

This operator $\mathrm{I}_{\mathrm{Cl}}^0$ acts on functions from $H_0^1(\Omega)$ and preserves zero boundary values.

Occasionally we also require an interpolation operator for functions from $H^1(\Omega)$, i.e. without specified boundary values. To this end denote temporarily the set of boundary nodes by $\mathcal{N}_\Gamma$ and define

$$\mathrm{I}_{\mathrm{Cl}} v := \sum_{\underline{x}_j \in \mathcal{N}_\Omega \cup \mathcal{N}_\Gamma} P_j(v)(\underline{x}_j) \, \varphi_j.$$

For vector or matrix valued functions act componentwise again.

From now on, V_{Cl}^0 will always be the space of *vector* valued functions.

The interpolation error estimates on anisotropic triangulations are different to the isotropic case. Roughly speaking, the anisotropic elements have to be aligned with the anisotropy of the function in order to obtain sharp estimates. To this end we define an *alignment measure* which measures the alignment of mesh and function.

Definition 4.3 (Alignment measure) *Let $\underline{v} \in [H^1(\Omega)]^d$ be a vector valued function, and $\mathcal{T}$ be a triangulation. The* alignment measure $m_1(\cdot, \cdot)$ *is then defined by*

$$m_1(\underline{v}, \mathcal{T}) := \frac{\left(\sum_{T \in \mathcal{T}} h_{min,T}^{-2} \|\nabla \underline{v} \cdot \underline{\underline{C}}_T\|_T^2 \right)^{1/2}}{\|\nabla \underline{v}\|}. \tag{19}$$

For a matrix valued function $\underline{\underline{s}} = (s_{i,j})_{i,j=1}^3 \in [H^1(\Omega)]^{3\times 3}$ the definition is componentwise, i.e.

$$m_1(\underline{\underline{s}}, \mathcal{T}) := \frac{\left(\sum_{T \in \mathcal{T}} h_{min,T}^{-2} \sum_{i,j=1}^3 \|(\nabla s_{i,j})^\top \cdot \underline{\underline{C}}_T\|_T^2 \right)^{1/2}}{\left(\sum_{T \in \mathcal{T}} \sum_{i,j=1}^3 \|\nabla s_{i,j}\|_T^2 \right)^{1/2}}.$$

The *influence* of the alignment measure can be observed immediately in the interpolation estimates below and in the upper error bounds of Section 6.3. For a better understanding we discuss here the *behaviour* of the alignment measure. The structure of the matrix $\underline{\underline{C}}_T$ from (11) readily gives the crude bounds

$$1 \leq m_1(\underline{v}, \mathcal{T}) \leq \max_{T \in \mathcal{T}} \frac{h_{max,T}}{h_{min,T}} \qquad ,$$

where $h_{max,T} \equiv h_{1,T}$ temporarily denotes the largest element dimension. Although this bound is practically useless, it implies an interesting by-product for *isotropic* meshes. There

one concludes $m_1(\underline{v}, \mathcal{T}) \sim 1$, and the alignment measure merges with other constants and thus 'vanishes'.

For *anisotropic* meshes the term $\nabla \underline{v} \cdot \underline{\underline{C}}_T$ of (19) contains directional derivatives along the main anisotropic directions $\underline{p}_{i,T}$ of the element T (since $\underline{\underline{C}}_T = [\underline{p}_{1,T}, \underline{p}_{2,T}, \underline{p}_{3,T}]$, see (11)). Consider first anisotropic elements that are *aligned* with an anisotropic function $\underline{v}$. Then the *long* anisotropic element direction $\underline{p}_{1,T}$ is associated with a *small* directional derivative $\nabla \underline{v} \cdot \underline{p}_{1,T}$. Conversely, the short direction $\underline{p}_{3,T}$ has a comparatively large directional derivative $\nabla \underline{v} \cdot \underline{p}_{3,T}$. Consequently the numerator and denominator of $m_1(\underline{v}, \mathcal{T})$ will be balanced, and $m_1(\underline{v}, \mathcal{T}) \sim 1$. Supplementary details are given in [Kun02].

If the anisotropic mesh is *not aligned* with an anisotropic function $\underline{v}$ then similar considerations imply that the numerator and denominator of $m_1(\underline{v}, \mathcal{T})$ are no longer balanced, and thus $m_1(\underline{v}, \mathcal{T}) \gg 1$.

Summarizing, the better the anisotropic mesh $\mathcal{T}$ is aligned with an anisotropic function v, the smaller $m_1(\underline{v}, \mathcal{T})$ will be. This results in sharper error bounds.

Finally we state the interpolation estimates.

Lemma 4.4 (Clément interpolation estimates) *For all functions $\underline{v}^0 \in [H_0^1(\Omega)]^d$ and $\underline{v} \in [H^1(\Omega)]^d$ one has*

$$\sum_{T \in \mathcal{T}} h_{min,T}^{-2} \|\underline{v}^0 - \mathrm{I}_{\mathrm{Cl}}^0 \underline{v}^0\|_T^2 \quad \lesssim \quad m_1^2(\underline{v}^0, \mathcal{T}) \, \|\nabla \underline{v}^0\|^2 \tag{20}$$

$$\sum_{E \in \mathcal{E}} \frac{h_E}{h_{min,E}^2} \|\underline{v}^0 - \mathrm{I}_{\mathrm{Cl}}^0 \underline{v}^0\|_E^2 \quad \lesssim \quad m_1^2(\underline{v}^0, \mathcal{T}) \, \|\nabla \underline{v}^0\|^2 \tag{21}$$

$$\sum_{E \in \mathcal{E}} \frac{h_E}{h_{min,E}^2} \|\underline{v} - \mathrm{I}_{\mathrm{Cl}} \underline{v}\|_E^2 \quad \lesssim \quad m_1^2(\underline{v}, \mathcal{T}) \, \|\nabla \underline{v}\|^2 \tag{22}$$

$$\sum_{E \in \mathcal{E}} \frac{h_E}{h_{min,E}^2} \|\mathrm{I}_{\mathrm{Cl}} \underline{v} - \mathcal{M}_E \mathrm{I}_{\mathrm{Cl}} \underline{v}\|_E^2 \quad \lesssim \quad m_1^2(\underline{v}, \mathcal{T}) \, \|\nabla \underline{v}\|^2, \tag{23}$$

where $\mathcal{M}_E$ is the face mean operator, i.e., $\mathcal{M}_E v := |E|^{-1} \int_E v$.
For matrix valued functions $\underline{v}$ all inequalities hold likewise.

Proof: The proof of the estimates (20) and (21) is given in [Kun00, Section 3] for triangles and tetrahedra. For (22) and for other elements, the proof is similar, with minor adaptions only.

For the estimate (23) we first use the triangular inequality and the property $\|\mathcal{M}_E \underline{v}\|_E \leq \|\underline{v}\|_E$ to get successively

$$\begin{aligned}
\|\mathrm{I}_{\mathrm{Cl}} \underline{v} - \mathcal{M}_E \mathrm{I}_{\mathrm{Cl}} \underline{v}\|_E^2 &\leq & \|\mathrm{I}_{\mathrm{Cl}} \underline{v} - \underline{v}\|_E^2 + \|\underline{v} - \mathcal{M}_E \underline{v}\|_E^2 + \|\mathcal{M}_E(\underline{v} - \mathrm{I}_{\mathrm{Cl}} \underline{v})\|_E^2 \\
&\leq & 2\|\mathrm{I}_{\mathrm{Cl}} \underline{v} - \underline{v}\|_E^2 + \|\underline{v} - \mathcal{M}_E \underline{v}\|_E^2.
\end{aligned}$$

Consider first $\|\underline{v} - \mathcal{M}_E \underline{v}\|_E$ and any of the two tetrahedra that contain this face E. Since the function $\mathcal{M}_E \underline{v}$ is constant on the face E, we extend it to T (and use the same notation

$\mathcal{M}_E\underline{v}$ here). The anisotropic trace inequality of [Kun00, Lemma 1] gives

$$h_E^{1/2}\|\underline{v} - \mathcal{M}_E\underline{v}\|_E \lesssim \|\underline{v} - \mathcal{M}_E\underline{v}\|_T + \|\nabla(\underline{v} - \mathcal{M}_E\underline{v})\cdot\underline{C}_T\|_T = \|\underline{v} - \mathcal{M}_E\underline{v}\|_T + \|\nabla\underline{v}\cdot\underline{C}_T\|_T.$$

In order to bound $\|\underline{v} - \mathcal{M}_E\underline{v}\|_T$ we require an anisotropic Poincaré-like inequality. To derive it, consider the reference element $\bar{T}$ (with face $\bar{E}$) and the specific (isotropic) Poincaré inequality $\|\bar{w}\|_{\bar{T}} \lesssim \|\bar{\nabla}\bar{w}\|_{\bar{T}} + |\int_{\bar{E}}\bar{w}|$. The transformation to the actual element T then gives

$$\|\underline{w}\|_T \lesssim \|\nabla\underline{w}\cdot\underline{C}_T\|_T + h_E^{1/2}\left|\int_E\underline{w}\right| \qquad \forall\underline{w}\in[H^1(\Omega)]^d, E\subset\partial T,$$

see also the proof of [Kun00, Lemma 4]. Set $\underline{w} := \underline{v} - \mathcal{M}_E\underline{v}$ which implies $\int_E\underline{w} = \int_E\underline{v} - \mathcal{M}_E\underline{v} = \underline{0}$ and $\nabla\underline{w} = \nabla\underline{v}$. Combining all these relations eventually leads to

$$\|\underline{v} - \mathcal{M}_E\underline{v}\|_T \lesssim \|\nabla\underline{v}\cdot\underline{C}_T\|_T \qquad \text{and} \qquad h_E^{1/2}\|\underline{v} - \mathcal{M}_E\underline{v}\|_E \lesssim \|\nabla\underline{v}\cdot\underline{C}_T\|_T.$$

Finally sum over all faces $E\in\mathcal{E}$, employ the definition of the alignment measure m_1 and utilize the previous estimate (22) to obtain the desired inequality (23). ∎

4.3 Trace estimates

Here we collect the trace estimates used below.

Lemma 4.5 *Let $\bar{T}$ be the reference element $(0,1)^d$ (rectangle or hexahedron), fix the face $\bar{E}$ of $\bar{T}$ included in the plane $\bar{y}=0$. Then for all $v\in H^1(\bar{T})$, it holds*

$$\left|\int_{\bar{E}}v\right| \leq \left|\int_{\bar{T}}v\right| + \|\partial_2 v\|_{\bar{T}}. \tag{24}$$

Proof: By density it suffices to show the assertion for smooth functions v. We prove the assertion in 3D, the 2D case follows by taking $v(x,y,z) = v(x,y)$. Using the identity

$$v(x,0,z) = v(x,y,z) - \int_0^y\partial_2 v(x,t,z)\mathrm{d}t, \qquad \forall x,y,z\in(0,1),$$

and integrating this equality on x,y,z, we obtain

$$\int_0^1\int_0^1 v(x,0,z)\,\mathrm{d}x\mathrm{d}z = \int_{\bar{T}}v(x,y,z)\,\mathrm{d}x\mathrm{d}y\mathrm{d}z - \int_{\bar{T}}\int_0^y\partial_2 v(x,t,z)\mathrm{d}t\,\mathrm{d}x\mathrm{d}y\mathrm{d}z.$$

The first two terms evaluate to $\left|\int_{\bar{E}}v\right|$ and $\left|\int_{\bar{T}}v\right|$. The last term can be bounded by repeated applications of the Cauchy-Schwarz inequality, giving

$$\int_{\bar{T}}\int_0^y\partial_2 v(x,t,z)\mathrm{d}t\,\mathrm{d}x\mathrm{d}y\mathrm{d}z \leq \int_{\bar{T}}\sqrt{y}\left(\int_0^y|\partial_2 v(x,t,z)|^2\mathrm{d}t\right)^{1/2}\mathrm{d}x\mathrm{d}y\mathrm{d}z$$

$$\leq \int_{\bar{T}}\left(\int_0^1|\partial_2 v(x,t,z)|^2\mathrm{d}t\right)^{1/2}\mathrm{d}x\mathrm{d}y\mathrm{d}z \leq \left(\int_{\bar{T}}\int_0^1|\partial_2 v(x,t,z)|^2\,\mathrm{d}t\mathrm{d}x\mathrm{d}y\mathrm{d}z\right)^{1/2}$$

$$\leq \left(\int_{\bar{T}}|\partial_2 v(x,t,z)|^2\,\mathrm{d}x\mathrm{d}t\mathrm{d}z\right)^{1/2} = \|\partial_2 v\|_{\bar{T}}.$$

The triangle inequality finishes the proof.   ∎

Lemma 4.6 *Consider the reference pentahedron $\bar{T}$ with rectangular faces $\bar{E}_3$, $\bar{E}_4$, $\bar{E}_5$ (which are included in the planes $y = 0$, $x = 0$, and $x + y = 1$, respectively). Then one has for all $v \in H^1(\bar{T})$*

$$\left| \int_{\bar{E}_i} v \right| \lesssim \left| \int_{\bar{T}} v \right| + \sum_{k=1,2} \|\partial_k v\|_{\bar{T}}, \qquad \forall i = 3, 4, 5. \tag{25}$$

Proof: By density it suffices to show the assertion for smooth functions v. We extend v to the reference hexahedron $(0,1)^3$ as follows:

$$\tilde{v}(x, y, z) := \left\{ \begin{array}{ll} v(x, y, z) & \text{if } (x, y, z) \in \bar{T}, \\ v(1 - y, 1 - x, z) & \text{otherwise.} \end{array} \right.$$

This extension belongs to $H^1((0,1)^3)$ and satisfies

$$\int_{(0,1)^3} \tilde{v} = 2 \int_{\bar{T}} v, \qquad \text{and} \qquad \|\partial_1 \tilde{v}\|_{(0,1)^3}^2 = \|\partial_2 \tilde{v}\|_{(0,1)^3}^2 = \|\partial_1 v\|_{\bar{T}}^2 + \|\partial_2 v\|_{\bar{T}}^2.$$

Applying the estimate (24) of Lemma 4.5 to $\tilde{v} \in H^1((0,1)^3)$ and using the last two identities, we arrive at the desired estimate (25) for the faces $\bar{E}_3$ and $\bar{E}_4$.

In order to show (25) for the last rectangular face $\bar{E}_5$, apply the linear transformation $(x, y, z) \to (1 - x - y, x, z)$ that maps $\bar{T}$ onto itself such that $\bar{E}_5$ becomes the face $\bar{E}_3$. For the transformed function, relation (25) holds. The transformation back yields the desired inequality for $\bar{E}_5$.   ∎

5   Examples of finite elements

In this subsection we present a (nonexhaustive) list of finite element pairs fulfilling the theoretical assumptions of the previous sections. The table gives a brief overview of the element pairs.

Section	Type	spatial dim.	Elements	Remarks
5.1	nonconform	2D+3D	triangles, tetrahedra	standard CR space
5.2	nonconform	2D	rectangles	enriched CR space
5.3	nonconform	2D	rectangles	enriched CR space
5.4	nonconform	3D	pentahedra	
5.5	nonconform	3D	hexahedra	
5.6	conform	2D	triangles, rectangles	Bernardi-Fortin-Raugel

As in the standard theory, a finite element is denoted by a triplet $(T, \mathcal{P}, \Sigma)$, where T is a domain, $\mathcal{P}$ denotes a space of functions, and Σ is a set of functionals of $\mathcal{P}^*$, cf. [Cia78].

5.1   Crouzeix-Raviart elements I

For a triangulation of Ω consisting of *triangles* in 2D or of *tetrahedra* in 3D, we approximate the velocity in the Crouzeix-Raviart finite element space and the pressure in the space of piecewise constant functions, namely (cf. [CR73, GR86, ANS01b])

$$V_{\text{veloc}} \;:=\; \{\underline{v}_h \in [L^2(\Omega)]^d : \underline{v}_h|_T \in [\mathbb{P}^1]^d \; \forall T, \int_E [\![\underline{v}_h]\!]_E = \underline{0} \;\forall E\}, \tag{26}$$

$$Q_{\text{pre}} \;:=\; \{q_h \in L_0^2(\Omega) : q_h|_T \in \mathbb{P}^0 \;\forall T\}. \tag{27}$$

It was shown in Lemma 3.1 of [ANS01b] that this pair is stable independently of the aspect ratio of the elements T of the triangulation, which means that (G2) is valid. Since in this case we have $V_{\text{Cl}}^0 = [H_0^1(\Omega)]^d \cap V_{\text{veloc}}$, the assumption (G1) holds. The Crouzeix-Raviart elements are nonconforming and satisfy the condition (CR) by definition.

5.2   Crouzeix-Raviart elements II

Here we restrict ourselves to the 2D case and to a triangulation of Ω made of *rectangles*. Due to the condition (G1) we actually need to modify the finite element given in [ANS01a, ANS01b]. On the reference rectangle $\bar{T} = (0,1)^2$ we define

$$\bar{\mathbb{Q}}^{1+} \;:=\; \text{span }\{1, \bar{x}, \bar{y}, \bar{x}\bar{y}, \bar{y}^2\}.$$

As degree of freedom (i.e. functionals of Σ) we take

$$\bar{l}_i(q) := \int_{\bar{E}_i} q, i = 1, \dots, 4, \qquad \bar{l}_5(q) := \int_{\bar{T}} \bar{q}_5 q,$$

where $\bar{E}_i$ are the four edges of $\bar{T}$, and $\bar{q}_5$ is the polynomial defined by

$$\bar{q}_5(\bar{x}, \bar{y}) := 3(2\bar{x} - 1)(2\bar{y} - 1).$$

One readily checks that the triplet $(\bar{T}, \bar{\mathbb{Q}}^{1+}, \{\bar{l}_i\}_{i=1}^5)$ is a finite element whose associated basis is given by $\{\bar{q}_i\}_{i=1}^5$, where

$$\begin{array}{llll}
\bar{q}_1(\bar{x}, \bar{y}) &:=& 1 - 4\bar{y} + 3\bar{y}^2, & \bar{q}_2(\bar{x}, \bar{y}) \;:=\; -2\bar{y} + 3\bar{y}^2, \\
\bar{q}_3(\bar{x}, \bar{y}) &:=& \frac{1}{2} - \bar{x} + 3\bar{y} - 3\bar{y}^2, & \bar{q}_4(\bar{x}, \bar{y}) \;:=\; -\frac{1}{2} + \bar{x} + 3\bar{y} - 3\bar{y}^2.
\end{array}$$

The edges are $\bar{E}_1 = (0,1) \times \{0\}$, $\bar{E}_2 = (0,1) \times \{1\}$, $\bar{E}_3 = \{0\} \times (0,1)$ and $\bar{E}_4 = \{1\} \times (0,1)$.

The finite element $(T, \mathbb{Q}^{1+}, \{l_i\}_{i=1}^5)$ on the actual anisotropic rectangle T is obtained by a standard affine transformation from $(\bar{T}, \bar{\mathbb{Q}}^{1+}, \{\bar{l}_i\}_{i=1}^5)$ such that $\bar{y}$ is mapped onto the stretching direction of the rectangle.[2]

---

[2]Note that the degrees of freedom l_i of the actual element become *mean* integrals (over E or T).

Now we define the approximation velocity space by

$$V_{\text{veloc}} := \{\underline{v}_h \in [L^2(\Omega)]^2 : \underline{v}_h|_T \in [\mathbb{Q}^{1+}]^2 \; \forall T, \int_E [\![\underline{v}_h]\!]_E = \underline{0} \; \forall E\}, \tag{28}$$

and take Q_{pre} as above, cf. (27).

Next we check the conditions on the elements. For the ease of the description, assume an axiparallel mesh, and define the auxiliary space

$$V_{\text{Apel}} := \{\underline{v}_h \in [L^2(\Omega)]^2 : \underline{v}_h|_T \in [\text{span}\{1, x, y, y^2\}]^2 \; \forall T, \int_E [\![\underline{v}_h]\!]_E = 0 \; \forall E\},$$

which has been introduced in [ANS01a, ANS01b].

The first condition (G1) clearly holds: For rectangles, V_{Cl}^0 consists of continuous and piecewise bilinear functions. (Note that (G1) is violated for V_{Apel}; therefore we had to enlarge the velocity space.)

Moreover by Lemma 6 of [ANS01a] and Lemma 3.1 of [ANS01b] the pair $(V_{\text{Apel}}, Q_{\text{pre}})$ is stable if for any rectangle T of the triangulation, the vector $p_{1,T}$ is parallel to the y-axis (i.e. the largest edges are parallel to the y-axis). As $V_{\text{Apel}} \subset \bar{V}_{\text{veloc}}$, (G2) holds under the same assumption on the mesh.

Finally, condition (CR) is satisfied trivially.

5.3   Crouzeix-Raviart elements III

Here we make the same restriction as in the previous section, i.e., we consider the 2D case and a triangulation of Ω made of *rectangles*. For the previous element, the local velocity space $V_{\text{veloc}}|_T$ depends on the stretching direction of the rectangle T. Here we modify the element such that this dependence on the directionality is removed.

Consider the reference rectangle $\bar{T} = (0,1)^2$, set $\bar{\mathcal{P}} := \mathbb{P}^2$, and define the degrees of freedom (with the same notation as before) by

$$\bar{l}_i(q) := \int_{\bar{E}_i} q, i = 1, 2, 3, 4, \qquad \bar{l}_5(q) := \int_{\bar{T}} q\bar{q}_5, \qquad \bar{l}_6(q) := \int_{\bar{T}} q,$$

with $\bar{q}_5$ as above. One easily checks that the triplet $(\bar{T}, \bar{\mathcal{P}}, \{\bar{l}_i\}_{i=1}^6)$ is a finite element whose associated basis is given by $\{\bar{q}_i\}_{i=1}^6$, with

$$\begin{array}{lll}
\bar{q}_1(\bar{x}, \bar{y}) := 1 - 4\bar{y} + 3\bar{y}^2, & \bar{q}_2(\bar{x}, \bar{y}) := -2\bar{y} + 3\bar{y}^2, & \bar{q}_3(\bar{x}, \bar{y}) := 1 - 4\bar{x} + 3\bar{x}^2 \\
\bar{q}_4(\bar{x}, \bar{y}) := -2\bar{x} + 3\bar{x}^2, & \bar{q}_5(\bar{x}, \bar{y}) := (2\bar{x} - 1)(2\bar{y} - 1) & \bar{q}_6(\bar{x}, \bar{y}) := 6(\bar{x} - \bar{x}^2 + \bar{y} - \bar{y}^2) - 1.
\end{array}$$

On a stretched rectangle T we take the finite element $(T, \mathbb{P}^2, \{l_i\}_{i=1}^6)$ obtained by a standard affine transformation from $\bar{T}$ to T, i.e. $q_i(x, y) = \bar{q}_i(\bar{x}, \bar{y})$ and $l_i(q) = \bar{l}_i(\bar{q})$.

The approximate velocity space is given by

$$\begin{aligned}
V_{\text{veloc}} & := [V_{\text{veloc}}^s]^2, \\
V_{\text{veloc}}^s & := \{v_h \in L^2(\Omega) : v_h|_T \in \mathbb{P}^2 \; \forall T, \int_E [\![v_h]\!]_E = 0 \; \forall E\},
\end{aligned} \tag{29}$$

and use Q_{pre} as defined by (27).

To prove the stability of this pair, for any $v \in H^1(\Omega)$ we define an interpolant $\mathrm{I}_{\mathrm{CR}}^{\mathrm{rect}}(v)$ of Crouzeix-Raviart's type as follows:

$$\mathrm{I}_{\mathrm{CR}}^{\mathrm{rect}}(v)|_T := \sum_{i=1}^{4} \frac{1}{|E_i|} \left(\int_{E_i} v \right) q_i + \frac{1}{|T|} \left(\int_T v \right) q_6, \qquad \forall T.$$

We now prove the following result:

Lemma 5.1 *For any $v \in H_0^1(\Omega)$, its interpolant $\mathrm{I}_{\mathrm{CR}}^{\mathrm{rect}}(v)$ belongs to V_{veloc}^s and satisfies*

$$\int_T \partial_j \mathrm{I}_{\mathrm{CR}}^{\mathrm{rect}}(v) = \int_T \partial_j v \qquad \forall T, \ j = 1, 2. \tag{30}$$

as well as

$$|\mathrm{I}_{\mathrm{CR}}^{\mathrm{rect}}(v)|_{1,\Omega} \leq |v|_{1,\Omega}. \tag{31}$$

Proof: The first assertion follows from Green's formula on any rectangle T and the property

$$\int_{E_i} \mathrm{I}_{\mathrm{CR}}^{\mathrm{rect}}(v) = \int_{E_i} v, \qquad i = 1, 2, 3, 4,$$

which is a direct consequence of the definition of $\mathrm{I}_{\mathrm{CR}}^{\mathrm{rect}}(v)$.

For the second assertion we remark that for any rectangle T by the affine transformation describe above, we have

$$\overline{\mathrm{I}_{\mathrm{CR}}^{\mathrm{rect}}(v)} = \overline{\mathrm{I}_{\mathrm{CR}}^{\mathrm{rect}}}(\bar{v}).$$

For any constant function $\bar{m} \in \mathbb{P}^0(\bar{T})$ one derives $\overline{\mathrm{I}_{\mathrm{CR}}^{\mathrm{rect}}}(\bar{v} - \bar{m}) = \overline{\mathrm{I}_{\mathrm{CR}}^{\mathrm{rect}}}(\bar{v}) - \bar{m}$ using the definition of $\mathrm{I}_{\mathrm{CR}}^{\mathrm{rect}}(v)$ and the identity $\bar{q}_6 + \sum_{i=1}^{4} \bar{q}_i \equiv 1$. Therefore we have $\partial_j \overline{\mathrm{I}_{\mathrm{CR}}^{\mathrm{rect}}}(\bar{v}) = \partial_j \overline{\mathrm{I}_{\mathrm{CR}}^{\mathrm{rect}}}(\bar{v} - \bar{m})$, for $j = 1, 2$. Set now $\bar{m} := |\bar{T}|^{-1} \int_{\bar{T}} \bar{v}$ and observe that $\bar{q}_3$ and $\bar{q}_4$ do not depend on $\bar{y}$ which implies

$$\partial_2 \overline{\mathrm{I}_{\mathrm{CR}}^{\mathrm{rect}}}(\bar{v}) = \partial_2 \overline{\mathrm{I}_{\mathrm{CR}}^{\mathrm{rect}}}(\bar{v} - \bar{m}) = \sum_{i=1,2} \frac{1}{|\bar{E}_i|} \left(\int_{\bar{E}_i} (\bar{v} - \bar{m}) \right) \partial_2 \bar{q}_i.$$

Now employ Lemma 4.5 to obtain

$$\|\partial_2 \overline{\mathrm{I}_{\mathrm{CR}}^{\mathrm{rect}}}(\bar{v})\|_{\bar{T}} \lesssim \|\partial_2 \bar{v}\|_{\bar{T}}.$$

Since $\bar{x}$ and $\bar{y}$ play a symmetric role, we similarly obtain $\|\partial_1 \overline{\mathrm{I}_{\mathrm{CR}}^{\mathrm{rect}}}(\bar{v})\|_{\bar{T}} \leq \|\partial_1 \bar{v}\|_{\bar{T}}$. For axiparallel rectangles the transformation back immediately yields

$$\|\partial_j \mathrm{I}_{\mathrm{CR}}^{\mathrm{rect}}(v)\|_T \leq \|\partial_j v\|_T, \text{ for } j = 1, 2,$$

and consequently the desired estimate (31). Non-axiparallel rectangles can be obtained from axiparallel ones by a simple rotation which leaves the H^1 seminorm unchanged. Thus (31) is proven there as well. ∎

Corollary 5.2 *The above pair $(V_{\text{veloc}}, Q_{\text{pre}})$ satisfies the uniform inf-sup condition.*

Proof: The arguments of Lemma 3.1 of [ANS01b] (taking as Fortin's operator $\mathrm{I}_{\text{CR}}^{\text{rect}}(\underline{u})$, defined componentwise) show that the property (30) and the estimate (31) are sufficient to guarantee the uniform inf-sup condition. ∎

Summarizing, we have build a pair based on a triangulation made of rectangles satisfying the assumptions (G1), (G2) and (CR).

5.4   Modified Crouzeix-Raviart elements on pentahedra

We restrict ourselves to the 3D case and to a triangulation of Ω made of rectangular *pentahedra*. We want to build a nonconforming approximation of V. Due to the condition (G1) we need to modify the finite element given in [ANS01a, ANS01b]. Indeed on a pentahedron T the velocity space has to contain the space spanned by $1, \bar{x}, \bar{y}, \bar{z}, \bar{x}\bar{z}, \bar{y}\bar{z}$, which is not the case of the space introduced in [ANS01a, ANS01b]. In view of the condition (CR) in the reference pentahedron $\bar{T}$, we then need to construct a finite element whose set $\bar{\Sigma}$ of degrees of freedom contains the mean on the five faces.

Now we take $\bar{\mathcal{P}} := \mathbb{P}^2$ and $\bar{\Sigma} := \{\bar{l}_i\}_{i=1}^{10}$ defined by

$$\bar{l}_i(p) := \int_{\bar{E}_i} p, \text{ for } i = 1, \ldots, 5, \qquad \bar{l}_6(p) := \int_{\bar{T}} p, \qquad \bar{l}_{i+6}(p) := \int_{\bar{T}} p\tilde{q}_i, \text{ for } i = 1, 2, 3, 4,$$

where

$$\begin{aligned}
\tilde{q}_1(\bar{x}, \bar{y}, \bar{z}) &:= 1 - 3\bar{x} - 2\bar{z} + 6\bar{x}\bar{z}, & \tilde{q}_2(\bar{x}, \bar{y}, \bar{z}) &:= 1 - 3\bar{y} - 2\bar{z} + 6\bar{y}\bar{z}, \\
\tilde{q}_3(\bar{x}, \bar{y}, \bar{z}) &:= 1 - 4\bar{x} - 2\bar{y} + 6\bar{x}\bar{y} + 3\bar{x}^2, & \tilde{q}_4(\bar{x}, \bar{y}, \bar{z}) &:= 2\bar{x} - 2\bar{y} - 3\bar{x}^2 + 3\bar{y}^2.
\end{aligned}$$

The above choice is motivated by the fact that $\bar{l}_i(\tilde{q}_j) = 0$ for $i = 1, \cdots, 6, j = 1, 2, 3, 4$.

As before one easily shows that the triplet $(\bar{T}, \mathbb{P}^2, \{\bar{l}_i\}_{i=1}^{10})$ is a finite element. Enumerate the faces $\bar{E}_i$ of $\bar{T}$ such that $\bar{E}_1, \bar{E}_2, \bar{E}_3, \bar{E}_4, \bar{E}_5$ are contained in the planes $\bar{z} = 0$, $\bar{z} = 1$, $\bar{y} = 0$, $\bar{x} = 0$ and $\bar{x} + \bar{y} = 1$, respectively. There exists an associated basis $\{\bar{q}_i\}_{i=1}^{10}$; here we need to specify the first six functions:

$$\begin{aligned}
\bar{q}_1(\bar{x}, \bar{y}, \bar{z}) &= 2(1 - 4\bar{z} + 3\bar{z}^2), & \bar{q}_4(\bar{x}, \bar{y}, \bar{z}) &= 1 - 6\bar{x} + 6\bar{x}^2, \\
\bar{q}_2(\bar{x}, \bar{y}, \bar{z}) &= 2(-2\bar{z} + 3\bar{z}^2), & \bar{q}_5(\bar{x}, \bar{y}, \bar{z}) &= (1 - 6(\bar{x} - \bar{x}^2 + \bar{y} - \bar{y}^2 - 2\bar{x}\bar{y}))/\sqrt{2}, \\
\bar{q}_3(\bar{x}, \bar{y}, \bar{z}) &= 1 - 6\bar{y} + 6\bar{y}^2, & \bar{q}_6(\bar{x}, \bar{y}, \bar{z}) &= 24(\bar{x} - \bar{x}^2 + \bar{y} - \bar{y}^2 - \bar{x}\bar{y}) + 12(\bar{z} - \bar{z}^2) - 6.
\end{aligned}$$

The main interest is that $\bar{q}_1, \bar{q}_2$ do not depend on $\bar{x}, \bar{y}$, and conversely $\bar{q}_3, \bar{q}_4, \bar{q}_5$ do not depend on $\bar{z}$.

Consider now the actual (anisotropic) pentahedron T which can be obtained from the reference pentahedron by an affine transformation, cf. Section 3.3. In this way also the finite element $(T, \mathcal{P}, \Sigma)$ is defined, i.e. one has $q_i(x, y, z) = \bar{q}_i(\bar{x}, \bar{y}, \bar{z})$ and $l_i(q) = \bar{l}_i(\bar{q})$.

At this stage we define the approximation velocity space V_{veloc} by

$$\begin{aligned}
V_{\text{veloc}} &:= [V_{\text{veloc}}^s]^3, \\
V_{\text{veloc}}^s &:= \{v_h \in L^2(\Omega) : v_h|_T \in \mathbb{P}^2 \; \forall T, \int_E [\![v_h]\!]_E = 0 \; \forall E\},
\end{aligned}$$

and define the approximation pressure space Q_{pre} again by (27). By construction the conditions (G1) and (CR) hold. Let us now check that the above pair is stable under the assumption that for any pentahedron T its triangular basis is isotropic (which is a reasonable assumption).

As before for any function $v \in H^1(\Omega)$ we define its interpolant $\text{I}_{\text{CR}}^{\text{pent}}(v)$:

$$\text{I}_{\text{CR}}^{\text{pent}}(v)|_T := \sum_{i=1}^{5} \frac{|\bar{E}_i|}{|E_i|} \left(\int_{E_i} v \right) q_i + \frac{|\bar{T}|}{|T|} \left(\int_T v \right) q_6, \forall T.$$

We remark that $\text{I}_{\text{CR}}^{\text{pent}}(v)$ belongs to V_{veloc}^s for all $v \in H_0^1(\Omega)$ since for any T, one has

$$\int_{E_i} \text{I}_{\text{CR}}^{\text{pent}}(v) = \int_{E_i} v, \text{ for } i = 1, \ldots, 5. \tag{32}$$

Again this identity and the aforementioned properties of $\bar{q}_i$, $i = 1, \ldots, 6$, allow to prove

Lemma 5.3 *For any $v \in H_0^1(\Omega)$, the interpolant $\text{I}_{\text{CR}}^{\text{pent}}(v)$ satisfies*

$$\int_T \partial_j \text{I}_{\text{CR}}^{\text{pent}}(v) = \int_T \partial_j v \qquad \forall T, \ j = 1, 2, 3. \tag{33}$$

Furthermore, if all pentahedra T have isotropic *triangular faces then*

$$|\text{I}_{\text{CR}}^{\text{pent}}(v)|_{1,\Omega} \lesssim |v|_{1,\Omega}. \tag{34}$$

Proof: The first assertion follows from Green's formula and property (32).

For the second assertion we remark that for any pentahedron T by the affine transformation mentioned above, we have

$$\overline{\text{I}_{\text{CR}}^{\text{pent}}(v)} = \overline{\text{I}_{\text{CR}}^{\text{pent}}}(\bar{v}).$$

Thanks to the particular form of the $\bar{q}_i$, $i = 1, \ldots, 6$, one has $\overline{\text{I}_{\text{CR}}^{\text{pent}}}(1) \equiv 1$, and thus $\overline{\text{I}_{\text{CR}}^{\text{pent}}}(\bar{v} - \bar{m}) = \overline{\text{I}_{\text{CR}}^{\text{pent}}}(\bar{v}) - \bar{m}$, for any constant function $\bar{m}$. Set $\bar{m} := |\bar{T}|^{-1} \int_{\bar{T}} \bar{v}$ and recall that $\bar{q}_1$ and $\bar{q}_2$ do not depend on $\bar{x}$ or $\bar{y}$. This yields

$$\partial_j \overline{\text{I}_{\text{CR}}^{\text{pent}}}(\bar{v}) = \partial_j \overline{\text{I}_{\text{CR}}^{\text{pent}}}(\bar{v} - \bar{m}) = \sum_{i=3}^{5} \left(\int_{\bar{E}_i} (\bar{v} - \bar{m}) \right) \partial_j \bar{q}_i, \qquad \text{for } j = 1, 2.$$

Therefore by Lemma 4.6 we obtain

$$\|\partial_j \overline{\text{I}_{\text{CR}}^{\text{pent}}}(\bar{v})\|_{\bar{T}} \lesssim \sum_{k=1,2} \|\partial_k \bar{v}\|_{\bar{T}}, \qquad \text{for } j = 1, 2.$$

For the third derivative utilize that $\bar{q}_3, \bar{q}_4, \bar{q}_5$ do not depend on $\bar{z}$ to obtain

$$\partial_3 \overline{\text{I}_{\text{CR}}^{\text{pent}}}(\bar{v}) = \partial_3 \overline{\text{I}_{\text{CR}}^{\text{pent}}}(\bar{v} - \bar{m}) = \sum_{i=1,2} \left(\int_{\bar{E}_i} (\bar{v} - \bar{m}) \right) \partial_3 \bar{q}_i.$$

Therefore by a slight modification of Lemma 4.5 we get $\|\partial_3 \overline{\mathrm{I}_{\mathrm{CR}}^{\mathrm{pent}}}(\bar{v})\|_{\bar{T}} \lesssim \|\partial_3 \bar{v}\|_{\bar{T}}$.

When going back to the original element T, we use similar arguments as in the previous section. Start with an axiparallel pentahedron. If the triangular faces are isotropic one can conclude

$$\|\partial_j \mathrm{I}_{\mathrm{CR}}^{\mathrm{pent}}(v)\|_T \;\lesssim\; \sum_{k=1,2} \|\partial_k v\|_T, \text{ for } j = 1, 2;$$

$$\|\partial_3 \mathrm{I}_{\mathrm{CR}}^{\mathrm{pent}}(v)\|_T \;\lesssim\; \|\partial_3 v\|_T,$$

which directly imply the requested estimate. For a non-axiparallel pentahedron employ the aforementioned rotation argument to achieve the same result. ∎

As in the previous subsection this lemma allows to conclude that the above pair $(V_{\mathrm{veloc}}, Q_{\mathrm{pre}})$ satisfies the uniform inf-sup condition under the above assumption.

5.5   Modified Crouzeix-Raviart elements on hexahedra

Here we consider the 3D case and a triangulation of Ω made of rectangular *hexahedra*. Inspired from the above subsection and the condition (G1), on the reference hexahedron $\bar{T} = (0,1)^3$, we take $\bar{\mathcal{P}} := \mathbb{P}^2 + \mathrm{span}\{\bar{x}\bar{y}\bar{z}\}$ and $\bar{\Sigma} := \{\bar{l}_i\}_{i=1}^{11}$ defined by

$$\bar{l}_i(p) := \int_{\bar{E}_i} p, \text{ for } i = 1, \ldots, 6, \qquad \bar{l}_7(p) := \int_{\bar{T}} p, \qquad \bar{l}_{i+7}(p) := \int_{\bar{T}} p\tilde{q}_i, \text{ for } i = 1, 2, 3, 4,$$

where

$$\begin{aligned}
\tilde{q}_1(\bar{x}, \bar{y}, \bar{z}) &:= 1 - 2\bar{x} - 2\bar{z} + 4\bar{x}\bar{z}, & \tilde{q}_2(\bar{x}, \bar{y}, \bar{z}) &:= 1 - 2\bar{y} - 2\bar{z} + 4\bar{y}\bar{z}, \\
\tilde{q}_3(\bar{x}, \bar{y}, \bar{z}) &:= 1 - 2\bar{x} - 2\bar{y} + 4\bar{x}\bar{y}, & \tilde{q}_4(\bar{x}, \bar{y}, \bar{z}) &:= 1 - \bar{x} - \bar{y} - \bar{z} + 4\bar{x}\bar{y}\bar{z}.
\end{aligned}$$

The above choice is motivated by the fact that $\bar{l}_i(\tilde{q}_j) = 0$ for $i = 1, \cdots, 7, j = 1, 2, 3, 4$.

As before the triplet $(\bar{T}, \bar{\mathcal{P}}, \{\bar{l}_i\}_{i=1}^{11})$ is a finite element. Denote the faces $\bar{E}_1, \ldots, \bar{E}_6$ such that they are included in the planes, $\bar{z} = 0$, $\bar{z} = 1$, $\bar{y} = 0$, $\bar{y} = 1$, $\bar{x} = 0$, $\bar{x} = 1$, respectively. Then there exists an associated basis $\{\bar{q}_i\}_{i=1}^{11}$ whose first six entries are of particular interest, and given by

$$\begin{aligned}
\bar{q}_1(\bar{x}, \bar{y}, \bar{z}) &= \bar{h}(\bar{z}) & \bar{q}_3(\bar{x}, \bar{y}, \bar{z}) &= \bar{h}(\bar{y}) & \bar{q}_5(\bar{x}, \bar{y}, \bar{z}) &= \bar{h}(\bar{x}) \\
\bar{q}_2(\bar{x}, \bar{y}, \bar{z}) &= \bar{h}(1 - \bar{z}) & \bar{q}_4(\bar{x}, \bar{y}, \bar{z}) &= \bar{h}(1 - \bar{y}) & \bar{q}_6(\bar{x}, \bar{y}, \bar{z}) &= \bar{h}(1 - \bar{x}),
\end{aligned}$$

where we have set $\bar{h}(t) := -2t + 3t^2$. Again the distinct feature is that $\bar{q}_1, \bar{q}_2$ depend only on $\bar{z}$, that $\bar{q}_3, \bar{q}_4$ depend only on $\bar{y}$, and $\bar{q}_5, \bar{q}_6$ depend only on $\bar{x}$. The finite element $(T, \mathcal{P}, \Sigma)$ on the actual hexahedron T is obtained by the usual affine transformation.

To define the pair $(V_{\mathrm{veloc}}, Q_{\mathrm{pre}})$, set[3]

$$V_{\mathrm{veloc}} := \left\{ \underline{v}_h \in [L^2(\Omega)]^3 : \underline{v}_h|_T \in [\mathbb{P}^2 + \mathrm{span}\{xyz\}]^3 \ \forall T, \int_E [\![\underline{v}_h]\!]_E = \underline{0} \ \forall E \right\},$$

---

[3]For the ease of notation, the definition of V_{veloc} is given for axiparallel meshes. Otherwise the $\mathrm{span}\{xyz\}$ has to be replaced by $\mathrm{span}\{\bar{x}\bar{y}\bar{z} \circ F_T^{-1}\}$, with F_T being the affine transformation from $\bar{T}$ to T.

and utilize Q_{pre} defined by (27). With a similar analysis as before one proves the stability of this element pair without any assumption on the mesh. Furthermore this pair satisfies (G1) and (CR) by definition.

Now we present a family of *conforming* elements which satisfies the assumptions (G1) and (G2).

5.6 Bernardi-Fortin-Raugel elements

The Bernardi-Fortin-Raugel elements yield a *conforming* discretization. Here we restrict ourselves to the 2D case and to a triangulation of Ω made of *triangles* or *rectangles*. The discrete pressure space Q_{pre} is the space of piecewise constant functions defined by (27), and the approximate velocity space is defined by (cf. [GR86, AN])

$$V_{\text{veloc}} := \{\underline{v}_h \in [H_0^1(\Omega)]^2 : \underline{v}_h|_T \in \mathcal{P}_T \ \forall T\}. \tag{35}$$

To define the local space $\mathcal{P}_T$ properly, start with triangular elements and consider an edge $E_i \subset \partial T$. Then let $\underline{p}_{E_i}$ be the edge bubble function 'in the direction of the normal vector' $\underline{n}_{E_i}$, i.e.

$$\underline{p}_{E_i} := \underline{n}_{E_i} b_{E_i,T}$$

(recall the definition of the edge bubble function $b_{E_i,T}$ from Section 4.1). The local space $\mathcal{P}_T$ then consists of linear functions enriched by the 'normal vector edge bubble functions' from above, namely

$$\mathcal{P}_T := [\mathbb{P}^1]^2 \oplus \text{span}\{\underline{p}_{E_i}\}_{i=1}^3.$$

For rectangular elements proceed similarly. Set again $\underline{p}_{E_i} := \underline{n}_{E_i} b_{E_i,T}$, where $b_{E_i,T}$ is of course an edge bubble function for the rectangle T. The local space $\mathcal{P}_T$ then becomes

$$\mathcal{P}_T := [\mathbb{Q}^1]^2 \oplus \text{span}\{\underline{p}_{E_i}\}_{i=1}^4.$$

For both elements, condition (G1) is fulfilled by definition. The stability of the Bernardi-Fortin-Raugel element is shown in [AN] for some families of meshes, i.e. assumption (G2) is satisfied too.

6 Error estimators

6.1 Residual error estimators

The general philosophy of residual error estimators is to estimate an appropriate norm of the correct residual by terms that can be evaluated easier, and that involve the data at hand. To this end denote the *exact element residual* by

$$\underline{R}_T := \underline{f} - (-\Delta \underline{u}_h + \nabla p_h) \text{ on } T.$$

As it is common [Ver96], this exact residual is replaced by some finite dimensional approximation called *approximate element residual* $\underline{r}_T$,

$$\underline{r}_T \in \mathbb{P}^k(T) \text{ on } T.$$

Depending on the polynomial order k and the actual finite element, this approximation can be achieved by projecting either $\underline{f}$ alone or $\underline{R}_T$ as a whole.

Next, introduce the gradient jump in normal and tangential direction by

$$\underline{J}_{E,n} := \begin{cases} \llbracket (\nabla \underline{u}_h - p_h \mathrm{I}) \underline{n}_E \rrbracket_E & \text{for interior edges/faces} \\ \underline{0} & \text{for boundary edges/faces} \end{cases}$$

$$\underline{J}_{E,t} := \llbracket \nabla \underline{u}_h \, \underline{t}_E \rrbracket_E \qquad \text{for nonconforming 2D case}$$

$$\underline{J}_{E,t} := \llbracket \nabla \underline{u}_h \times \underline{n}_E \rrbracket_E \qquad \text{for nonconforming 3D case.}$$

For nonconforming discretizations the tangential jump does not vanish on boundary faces.

Definition 6.1 (Residual error estimator) *For a conforming discretization, the* local residual error estimators *is defined by*

$$\eta_T^2 := h_{min,T}^2 \|\underline{r}_T\|_T^2 + \|\mathrm{div}\, \underline{u}_h\|_T^2 + \sum_{E \subset \partial T} \frac{h_{min,T}^2}{h_E} \|\underline{J}_{E,n}\|_E^2.$$

For a nonconforming 2D discretization we set

$$\eta_T^2 := h_{min,T}^2 \|\underline{r}_T\|_T^2 + \|\mathrm{div}\, \underline{u}_h\|_T^2 + \sum_{E \subset \partial T} \frac{h_{min,T}^2}{h_E} \left(\|\underline{J}_{E,n}\|_E^2 + \|\underline{J}_{E,t}\|_E^2 \right),$$

while for a nonconforming 3D discretization the definition becomes

$$\eta_T^2 := h_{min,T}^2 \|\underline{r}_T\|_T^2 + \|\mathrm{div}\, \underline{u}_h\|_T^2 \; + \; \sum_{E \subset \partial T} \frac{h_{min,T}^2}{h_E} \left(\|\underline{J}_{E,n}\|_E^2 + \|\underline{J}_{E,t}\|_E^2 \right)$$

$$+ \sum_{E \subset \partial T, E \in \mathcal{E}_\square} \frac{h_{min,T}^2}{h_E \varrho(E)^2} \|\llbracket \underline{u}_h \rrbracket_E\|_E^2.$$

In the isotropic 3D case, *the last term containing* $\llbracket u_h \rrbracket_E$ *can be omitted.*

The global residual error estimators *is given by*

$$\eta^2 := \sum_{T \in \mathcal{T}} \eta_T^2.$$

Furthermore denote the local and global approximation terms *by*

$$\zeta_T^2 := \sum_{T' \subset \omega_T} h_{min,T'}^2 \|\underline{r}_{T'} - \underline{R}_{T'}\|_{T'}^2, \qquad \zeta^2 := \sum_{T \in \mathcal{T}} \zeta_T^2.$$

Note that in the 3D case, the jump of $\underline{u}_h$ is bounded by $\|[\![\underline{u}_h]\!]_E\|_E \lesssim \operatorname{diam}(E)\|\underline{J}_{E,t}\|_E$ due to Poincaré's inequality and the assumption (CR). For isotropic discretizations one has $\operatorname{diam}(E) \sim \varrho(E)$ and thus

$$\varrho(E)^{-1}\|[\![\underline{u}_h]\!]_E\|_E \sim \|\underline{J}_{E,t}\|_E \qquad \text{for } E \in \mathcal{E}_\square.$$

Therefore, in this case it is not necessary to add $\|[\![\underline{u}_h]\!]_E\|_E$ to the definition of η_T.

6.2 Proof of the lower error bound

The general framework of most of our exposition below is (more or less) standard (see [Ver96, DDP95] for the isotropic 2D counterpart). All 3D considerations seem to be novel. Recall further the notation for the velocity error $\underline{e} = \underline{u} - \underline{u}_h$ and the pressure error $\varepsilon = p - p_h$.

Theorem 6.2 (Local lower error bound) *Assume that one of the following cases holds: the discretization is 2D, or the discretization is 3D and is conforming, or the discretization is 3D, is nonconforming and is only composed of tetrahedra. Then for all elements T, the following local lower error bound holds:*

$$\eta_T \lesssim \|\nabla_T \underline{e}\|_{\omega_T} + \|\varepsilon\|_{\omega_T} + \zeta_T. \tag{36}$$

Proof: We start by bounding each of the residuals separately.

Element residual: Set $\underline{w}_T := \underline{r}_T b_T \in [H_0^1(T)]^d$ and integrate by parts to obtain

$$
\begin{aligned}
\int_T \underline{r}_T \cdot \underline{w}_T &= \int_T \underline{R}_T \cdot \underline{w}_T + \int_T (\underline{r}_T - \underline{R}_T) \cdot \underline{w}_T \\
&= \int_T (-\Delta(\underline{u} - \underline{u}_h) + \nabla(p - p_h)) \cdot \underline{w}_T + \int_T (\underline{r}_T - \underline{R}_T) \cdot \underline{w}_T \\
&= \int_T (\nabla \underline{e} - \varepsilon \mathrm{I}) : \nabla \underline{w}_T - \int_{\partial T} (\nabla \underline{e} - \varepsilon \mathrm{I})\underline{n} \cdot \underline{w}_T + \int_T (\underline{r}_T - \underline{R}_T) \cdot \underline{w}_T \\
&\leq (\|\nabla \underline{e}\|_T + \|\varepsilon\|_T)\|\nabla \underline{w}_T\|_T + \|\underline{r}_T - \underline{R}_T\|_T \|\underline{w}_T\|_T.
\end{aligned}
$$

The inverse inequalities (12), (13) and the obvious relation $\|\underline{w}_T\|_T \leq \|\underline{r}_T\|_T$ imply

$$\|\underline{r}_T\|_T \lesssim h_{min,T}^{-1}(\|\nabla \underline{e}\|_T + \|\varepsilon\|_T) + \|\underline{r}_T - \underline{R}_T\|_T. \tag{37}$$

Divergence: With d being the space dimension, one easily concludes

$$\|\operatorname{div} \underline{u}_h\|_T = \|\operatorname{div}(\underline{u} - \underline{u}_h)\|_T \leq \sqrt{d}\,\|\nabla(\underline{u} - \underline{u}_h)\|_T = \sqrt{d}\,\|\nabla \underline{e}\|_T. \tag{38}$$

Normal jump: For an interior edge/face E consider $\omega_E = T_1 \cup T_2$. Let us assume that $T \equiv T_1$. Recall that $\underline{J}_{E,n} \in [\mathbb{P}^k(E)]^d$ for some $k \in \mathbb{N}$ depending on the chosen finite element space. Set

$$\underline{w}_E := \mathrm{F}_{\mathrm{ext}}(\underline{J}_{E,n})b_E \in [H_0^1(\omega_E)]^d.$$

Partial integration on ω_E yields

$$\int_{\omega_E} \underline{f} \cdot \underline{w}_E = \int_{\omega_E} (-\Delta \underline{u} + \nabla p) \cdot \underline{w}_E = \int_{\omega_E} (\nabla \underline{u} - p\mathrm{I}) : \nabla \underline{w}_E - \int_{\partial \omega_E} (\nabla \underline{u} - p\mathrm{I})\underline{n} \cdot \underline{w}_E$$

$$= \int_{\omega_E} (\nabla \underline{u} - p\mathrm{I}) : \nabla \underline{w}_E.$$

By elementwise partial integration we further conclude

$$-\int_E \underline{J}_{E,n} \cdot \underline{w}_E = \sum_{i=1}^2 \int_{\partial T_i} (\nabla \underline{u}_h - p_h \mathrm{I})\underline{n} \cdot \underline{w}_E$$

$$= \int_{\omega_E} (\nabla \underline{u}_h - p_h \mathrm{I}) : \nabla \underline{w}_E - \sum_{i=1}^2 \int_{T_i} (-\Delta \underline{u}_h + \nabla p_h) \cdot \underline{w}_E$$

$$= -\int_{\omega_E} (\nabla \underline{e} - \varepsilon \mathrm{I}) : \nabla \underline{w}_E + \sum_{i=1}^2 \int_{T_i} (\underline{f} - (-\Delta \underline{u}_h + \nabla p_h)) \cdot \underline{w}_E$$

$$\leq (\|\nabla_{\mathcal{T}} \underline{e}\|_{\omega_E} + \|\varepsilon\|_{\omega_E}) \|\nabla \underline{w}_E\|_{\omega_E} + \sum_{i=1}^2 (\|\underline{r}_{T_i}\|_{T_i} + \|\underline{r}_{T_i} - \underline{R}_{T_i}\|_{T_i}) \|\underline{w}_E\|_{\omega_E}.$$

The inverse inequalities (14)–(16) and the previous bound (37) of $\|\underline{r}_{T_i}\|_{T_i}$ imply

$$\frac{h_{min,T}^2}{h_E} \|\underline{J}_{E,n}\|_E^2 \lesssim \|\nabla_{\mathcal{T}} \underline{e}\|_{\omega_E}^2 + \|\varepsilon\|_{\omega_E}^2 + h_{min,T}^2 \sum_{i=1}^2 \|\underline{r}_{T_i} - \underline{R}_{T_i}\|_{T_i}^2. \qquad (39)$$

For a Dirichlet boundary edge nothing needs to be done since $\underline{J}_{E,n} \equiv 0$ there.

Tangential jump (for nonconforming elements only): In the 2D case, set

$$\underline{w}_E := \mathrm{F}_{ext}(\underline{J}_{E,t}) b_E \in [H_0^1(\omega_E)]^2.$$

Partial integration for $\underline{u} \in [H^1(\omega_E)]^2, \underline{w}_E \in [H_0^1(\omega_E)]^2$ results in (see (5))

$$0 = \int_{\partial \omega_E} (\nabla \underline{u} \, \underline{t}) \cdot \underline{w}_E = -\int_{\omega_E} \nabla \underline{u} : \underline{\underline{\mathrm{curl}}} \, \underline{w}_E.$$

For $\underline{u}_h$ we integrate elementwise and obtain

$$-\int_E \underline{J}_{E,t} \cdot \underline{w}_E = \sum_{i=1}^2 \int_{\partial T_i} (\nabla \underline{u}_h \, \underline{t}) \cdot \underline{w}_E = \sum_{i=1}^2 \int_{T_i} \nabla \underline{u}_h : \underline{\underline{\mathrm{curl}}} \, \underline{w}_E$$

$$= \sum_{i=1}^2 \int_{T_i} \nabla (\underline{u}_h - \underline{u}) : \underline{\underline{\mathrm{curl}}} \, \underline{w}_E$$

$$\lesssim \|\nabla_{\mathcal{T}} \underline{e}\|_{\omega_E} \|\nabla \underline{w}_E\|_{\omega_E}.$$

The inverse inequalities (14) and (16) lead to

$$\frac{h_{min,T}^2}{h_E}\|\underline{J}_{E,t}\|_E^2 \;\lesssim\; \|\nabla_{\mathcal{T}}\,\underline{e}\,\|_{\omega_E}^2. \tag{40}$$

For a Dirichlet boundary edge the analysis is modified appropriately.

In the 3D case, we set

$$\underline{w}_E := \mathrm{F}_{\mathrm{ext}}(\underline{J}_{E,t})b_E \in [H_0^1(\omega_E)]^{3\times 3}.$$

The proof is the same as in 2D, using identity (6) instead of (5) for the partial integration and the inverse inequality (17).

Summarizing all results provides the desired local lower error bound (36).   ■

For a nonconforming 3D discretization we are unfortunately not able to estimate locally the contribution of the rectangular faces (Rectangular jump). But a global lower bound is available using the alignment measure.

Theorem 6.3 (Global lower error bound) *For 3D discretizations, the following global lower error bound holds:*

$$\sum_{T\in\mathcal{T}}\ \sum_{E\subset\partial T, E\in\mathcal{E}_\square} h_{min,T}^2 h_E^{-1}\varrho(E)^{-2}\|[\![\underline{u}_h]\!]_E\|_E^2 \lesssim m_1(\underline{e},\mathcal{T})^2\|\nabla_{\mathcal{T}}\,\underline{e}\,\|^2. \tag{41}$$

Proof: Start with hexahedral elements, and let $E\in\mathcal{E}_\square$ be an interior rectangular face with neighbours T_1 and T_2. Consider those two affine linear transformations that map the unit cube $(0,1)^3$ onto T_i, $i=1$ and 2, such that E corresponds to the same transformed face $\tilde{E} = \{0\}\times(0,1)^2$, say. Denote the transformation matrices temporarily by $\underline{\tilde{C}}_{T_1}$ and $\underline{\tilde{C}}_{T_2}$ and note that they can be obtained from $\underline{C}_{T_i}$ by a simple rotation, cf. Section 3.3. Correspondingly, let the transformed error functions $\underline{e}|_{T_i}$ be $\underline{\tilde{e}}_i$. Next, introduce the function

$$\tilde{\underline{v}}(\tilde{x},\tilde{y},\tilde{z}) := \underline{\tilde{e}}_1(\tilde{x},\tilde{y},\tilde{z}) - \underline{\tilde{e}}_2(\tilde{x},\tilde{y},\tilde{z}) \in H^1((0,1)^3)$$

and observe $\int_{\tilde{E}}\tilde{v} = 0$ due to the (CR) property of the discretization. This readily implies a Poincaré like inequality $\|\tilde{\underline{v}}\|_{H^1((0,1)^3)} \sim |\tilde{\underline{v}}|_{H^1((0,1)^3)}$. The standard trace inequality yields $\|\tilde{\underline{v}}\|_{L^2(\tilde{E})} \lesssim \|\tilde{\underline{v}}\|_{H^1((0,1)^3)} \sim |\tilde{\underline{v}}|_{H^1((0,1)^3)}$ and thus

$$\|\underline{\tilde{e}}_1 - \underline{\tilde{e}}_2\|_{L^2(\tilde{E})} \lesssim |\underline{\tilde{e}}_1 - \underline{\tilde{e}}_2|_{H^1((0,1)^3)} \le |\underline{\tilde{e}}_1|_{H^1((0,1)^3)} + |\underline{\tilde{e}}_2|_{H^1((0,1)^3)} \quad .$$

The transformation back to the original elements provide

$$\begin{aligned} h_E^{1/2}\|[\![\underline{u}_h]\!]_E\|_E = h_E^{1/2}\|\underline{e}|_{T_1} - \underline{e}|_{T_2}\|_{L^2(E)} &\lesssim \|\nabla\underline{e}\cdot\underline{\tilde{C}}_{T_1}\|_{T_1} + \|\nabla\underline{e}\cdot\underline{\tilde{C}}_{T_2}\|_{T_2}\\ &\lesssim \|\nabla\underline{e}\cdot\underline{C}_{T_1}\|_{T_1} + \|\nabla\underline{e}\cdot\underline{C}_{T_2}\|_{T_2} \end{aligned}$$

since $\underline{\tilde{\underline{C}}}_{T_i}$ and $\underline{C}_{T_i}$ differ only by a rotation. Apply this inequality to the left-hand side of (41) to conclude

$$\sum_{T\in\mathcal{T}}\sum_{E\subset\partial T, E\in\mathcal{E}_\square}h^2_{min,T}h_E^{-1}\varrho(E)^{-2}\|[\![\underline{u}_h]\!]_E\|_E^2 \lesssim \sum_{T\in\mathcal{T}}\sum_{E\subset\partial T, E\in\mathcal{E}_\square}h^2_{min,T}h_E^{-2}\varrho(E)^{-2}\sum_{T\subset\omega_E}\|\nabla\underline{e}\cdot\underline{\underline{C}}_T\|_T^2.$$

From $h_E\gtrsim h_{min,T}$ and $\varrho(E)\gtrsim h_{min,T}$ we further derive

$$\sum_{T\in\mathcal{T}}\sum_{E\subset\partial T, E\in\mathcal{E}_\square}h^2_{min,T}h_E^{-1}\varrho(E)^{-2}\|[\![\underline{u}_h]\!]_E\|_E^2 \lesssim \sum_{T\in\mathcal{T}}h_{min,T}^{-2}\|\nabla\underline{e}\cdot\underline{\underline{C}}_T\|_T^2 \lesssim m_1(\underline{e},\mathcal{T})^2\|\nabla_\mathcal{T}\,\underline{e}\|^2$$

by the definition of the alignment measure.

For rectangular faces of pentahedral elements proceed analogously.   ∎

Corollary 6.4 (Global lower error bound)   *For a 3D nonconforming triangulation consisting of pentahedra or hexahedra, the following global lower error bound holds:*

$$\sum_{T\in\mathcal{T}}\eta_T^2 \lesssim m_1(\underline{e},\mathcal{T})^2\|\nabla_\mathcal{T}\,\underline{e}\|^2.$$

6.3   Proof of the upper error bound

For the nonconforming 2D case we proceed similar to [DDP95], with the necessary adaptations due to the anisotropy of our discretization. The whole 3D analysis seems to be new. Basic steps are always partial integration, combined with Galerkin like orthogonalities and interpolation error estimates.

First we bound the pressure error (for conforming and nonconforming discretizations). The bound of the velocity error is divided in two parts since conforming and nonconforming discretizations are treated differently.

6.3.1   Error in the pressure

We start with an estimate of the pressure error that is valid for conforming and nonconforming elements.

Lemma 6.5 (Error in the pressure)   *There exists a function $\underline{v}_\varepsilon \in [H_0^1(\Omega)]^d$ depending on $\varepsilon = p - p_h$ such that the error in the pressure is bounded by*

$$\|\varepsilon\| \lesssim m_1(\underline{v}_\varepsilon,\mathcal{T})(\eta+\zeta)+\|\nabla_\mathcal{T}\,\underline{e}\|. \tag{42}$$

Proof: Since $\varepsilon\in L_0^2(\Omega)$, there exists a function $\underline{v}_\varepsilon\in[H_0^1(\Omega)]^d$ such that

$$\|\varepsilon\| \lesssim \frac{\int_\Omega \varepsilon\,\mathrm{div}\,\underline{v}_\varepsilon}{\|\nabla\underline{v}_\varepsilon\|},$$

cf. [GR86]. This inequality is equivalent to the continuous inf-sup condition, applied to the pressure error ε. Since the continuous inf-sup condition is not related to the discretization, the inequality constant is independent of any mesh anisotropy. Next, consider the Clément interpolant of $\underline{v}_\varepsilon$,

$$\mathrm{I}_{\mathrm{Cl}}^0 \underline{v}_\varepsilon \in V_{\mathrm{Cl}}^0 \subset [H_0^1(\Omega)]^d \cap V_{\mathrm{veloc}}.$$

By using the Galerkin orthogonality (10) and partial integration, we conclude

$$
\begin{aligned}
\int_\Omega \varepsilon \operatorname{div} \underline{v}_\varepsilon \ \overset{(10)}{=}\ & \int_\Omega \varepsilon \operatorname{div}(\underline{v}_\varepsilon - \mathrm{I}_{\mathrm{Cl}}^0 \underline{v}_\varepsilon) + \int_\Omega \nabla_{\mathcal{T}}\, \underline{e}\, : \nabla \mathrm{I}_{\mathrm{Cl}}^0 \underline{v}_\varepsilon \\
=\ & \int_\Omega (-\nabla \underline{u} + p\mathrm{I}) : \nabla(\underline{v}_\varepsilon - \mathrm{I}_{\mathrm{Cl}}^0 \underline{v}_\varepsilon) - \sum_{T \in \mathcal{T}} \int_T (-\nabla \underline{u}_h + p_h \mathrm{I}) : \nabla(\underline{v}_\varepsilon - \mathrm{I}_{\mathrm{Cl}}^0 \underline{v}_\varepsilon) \\
& + \int_\Omega \nabla_{\mathcal{T}}\, \underline{e}\, : \nabla \underline{v}_\varepsilon \\
=\ & -\int_\Omega (-\Delta \underline{u} + \nabla p) \cdot (\underline{v}_\varepsilon - \mathrm{I}_{\mathrm{Cl}}^0 \underline{v}_\varepsilon) + \int_{\partial\Omega} (-\nabla \underline{u} + p\mathrm{I})\underline{n} \cdot (\underline{v}_\varepsilon - \mathrm{I}_{\mathrm{Cl}}^0 \underline{v}_\varepsilon) \\
& + \sum_{T \in \mathcal{T}} \left\{ \int_T (-\Delta \underline{u}_h + \nabla p_h) \cdot (\underline{v}_\varepsilon - \mathrm{I}_{\mathrm{Cl}}^0 \underline{v}_\varepsilon) - \int_{\partial T} (-\nabla \underline{u}_h + p_h \mathrm{I})\underline{n} \cdot (\underline{v}_\varepsilon - \mathrm{I}_{\mathrm{Cl}}^0 \underline{v}_\varepsilon) \right\} \\
& + \int_\Omega \nabla_{\mathcal{T}}\, \underline{e}\, : \nabla \underline{v}_\varepsilon \\
=\ & -\sum_{T \in \mathcal{T}} \int_T (\underline{f} - (-\Delta \underline{u}_h + \nabla p_h)) \cdot (\underline{v}_\varepsilon - \mathrm{I}_{\mathrm{Cl}}^0 \underline{v}_\varepsilon) + \sum_{E \in \mathcal{E}} \int_E \underline{J}_{E,n} \cdot (\underline{v}_\varepsilon - \mathrm{I}_{\mathrm{Cl}}^0 \underline{v}_\varepsilon) \\
& + \int_\Omega \nabla_{\mathcal{T}}\, \underline{e}\, : \nabla \underline{v}_\varepsilon \\
\leq\ & \sum_{T \in \mathcal{T}} h_{min,T} \|\underline{R}_T\|_T\, h_{min,T}^{-1} \|\underline{v}_\varepsilon - \mathrm{I}_{\mathrm{Cl}}^0 \underline{v}_\varepsilon\|_T \\
& + \sum_{E \in \mathcal{E}} h_{min,E} h_E^{-1/2} \|\underline{J}_{E,n}\|_E\, h_{min,E}^{-1} h_E^{1/2} \|\underline{v}_\varepsilon - \mathrm{I}_{\mathrm{Cl}}^0 \underline{v}_\varepsilon\|_E \\
& + \|\nabla_{\mathcal{T}}\, \underline{e}\,\|\, \|\nabla \underline{v}_\varepsilon\|.
\end{aligned}
$$

The Cauchy–Schwarz inequality and the Clément interpolation results of Lemma 4.4 imply

$$
\begin{aligned}
\int_\Omega \varepsilon \operatorname{div} \underline{v}_\varepsilon \ \lesssim\ & \left(\sum_{T \in \mathcal{T}} h_{min,T}^2 \|\underline{R}_T\|_T^2 + \sum_{E \in \mathcal{E}} h_{min,E}^2 h_E^{-1} \|\underline{J}_{E,n}\|_E^2 \right)^{1/2} m_1(\underline{v}_\varepsilon, \mathcal{T}) \|\nabla \underline{v}_\varepsilon\| \\
& + \|\nabla_{\mathcal{T}}\, \underline{e}\,\|\, \|\nabla \underline{v}_\varepsilon\| \\
\lesssim\ & \left\{ (\eta + \zeta) m_1(\underline{v}_\varepsilon, \mathcal{T}) + \|\nabla_{\mathcal{T}}\, \underline{e}\,\| \right\} \|\nabla \underline{v}_\varepsilon\|
\end{aligned}
$$

which finishes the proof. ∎

6.3.2   Error in the velocity - Conforming case

Lemma 6.6 (Error in the velocity - Conforming case.) *Assume a* conform *discretization, and let* $\underline{v}_\varepsilon \in [H_0^1(\Omega)]^d$ *be the function from Lemma 6.5. Then the error in the velocity is bounded by*

$$\|\nabla_{\mathcal{T}}\,\underline{e}\,\| \;\lesssim\; \Big(m_1(\underline{e},\mathcal{T}) + m_1(\underline{v}_\varepsilon,\mathcal{T})^{1/2}\Big)(\eta + \zeta). \tag{43}$$

Proof: Note first that here the elementwise operators $\mathrm{div}_{\mathcal{T}}$ and $\nabla_{\mathcal{T}}$ are identical with the global operators div and ∇. Since $\underline{e} \in [H_0^1(\Omega)]^d$, one can utilize the Clément interpolant $\mathrm{I}_{\mathrm{Cl}}^0\underline{e} \in [H_0^1(\Omega)]^d \cap V_{\mathrm{veloc}}$ and the Galerkin orthogonality (10) for $\mathrm{I}_{\mathrm{Cl}}^0\underline{e}$. Then integrate by parts and employ the interpolation results to obtain

$$
\begin{aligned}
\|\nabla_{\mathcal{T}}\,\underline{e}\,\|^2 \;&=\; \int_\Omega (\nabla_{\mathcal{T}}\,\underline{e} - \varepsilon\mathrm{I}) : \nabla_{\mathcal{T}}\,\underline{e} + \int_\Omega \varepsilon\,\mathrm{div}_{\mathcal{T}}\underline{e} \\[4pt]
&\overset{(10)}{=} \int_\Omega (\nabla_{\mathcal{T}}\,\underline{e} - \varepsilon\mathrm{I}) : \nabla_{\mathcal{T}}\,(\underline{e} - \mathrm{I}_{\mathrm{Cl}}^0\underline{e}) - \int_\Omega \varepsilon\,\mathrm{div}_{\mathcal{T}}\underline{u}_h \\[4pt]
&\overset{(3),(4)}{=} \int_\Omega (-\Delta\underline{u} + \nabla p)\cdot(\underline{e} - \mathrm{I}_{\mathrm{Cl}}^0\underline{e}) - \int_{\partial\Omega}(-\nabla\underline{u} + p\mathrm{I})\underline{n}\cdot(\underline{e} - \mathrm{I}_{\mathrm{Cl}}^0\underline{e}) \\[4pt]
&\quad + \sum_{T\in\mathcal{T}}\Big\{\int_T (\Delta\underline{u}_h - \nabla p_h)\cdot(\underline{e} - \mathrm{I}_{\mathrm{Cl}}^0\underline{e}) - \int_{\partial T}(\nabla\underline{u}_h - p_h\mathrm{I})\underline{n}\cdot(\underline{e} - \mathrm{I}_{\mathrm{Cl}}^0\underline{e})\Big\} \\[4pt]
&\quad - \int_\Omega \varepsilon\,\mathrm{div}_{\mathcal{T}}\underline{u}_h \\[4pt]
&= \sum_{T\in\mathcal{T}}\int_T \underline{R}_T\cdot(\underline{e} - \mathrm{I}_{\mathrm{Cl}}^0\underline{e}) + \sum_{E\in\mathcal{E}}\int_E \underline{J}_{E,n}\cdot(\underline{e} - \mathrm{I}_{\mathrm{Cl}}^0\underline{e}) - \int_\Omega \varepsilon\,\mathrm{div}_{\mathcal{T}}\underline{u}_h.
\end{aligned}
$$

Invoke again the Cauchy–Schwarz inequality, the Clément interpolation inequalities (20), (21), and the bound of $\|\varepsilon\|$ from Lemma 6.5. Additionally employ the triangle inequality for the exact residual $\underline{R}_T$ as well as the obvious bound $\|\mathrm{div}_{\mathcal{T}}\underline{u}_h\| \leq \eta$ to obtain

$$
\begin{aligned}
\|\nabla_{\mathcal{T}}\,\underline{e}\,\|^2 \;&\lesssim\; (\eta+\zeta)\,m_1(\underline{e},\mathcal{T})\,\|\nabla_{\mathcal{T}}\,\underline{e}\,\| + \Big(m_1(\underline{v}_\varepsilon,\mathcal{T})(\eta+\zeta) + \|\nabla_{\mathcal{T}}\,\underline{e}\,\|\Big)\|\mathrm{div}_{\mathcal{T}}\underline{u}_h\| \\[4pt]
&\leq\; (\eta+\zeta)\,m_1(\underline{e},\mathcal{T})\,\|\nabla_{\mathcal{T}}\,\underline{e}\,\| + m_1(\underline{v}_\varepsilon,\mathcal{T})(\eta+\zeta)\eta + \eta\,\|\nabla_{\mathcal{T}}\,\underline{e}\,\|.
\end{aligned}
$$

Young's inequality and the trivial relation $1 \leq m_1(\cdot,\mathcal{T})$ provide the desired velocity error bound.   ∎

We remark that this proof is not exactly a special case of the nonconforming exposition below, although there are similarities.

The error bounds for the pressure and the velocity immediately yield the following main theorem.

Theorem 6.7 (Upper error bound - Conforming case.) *Assume a* conform *discretization, and let $\underline{v}_\varepsilon \in [H_0^1(\Omega)]^d$ be the function from Lemma 6.5. Then the error is bounded globally from above by*

$$\|\varepsilon\| + \|\nabla_{\mathcal{T}}\,\underline{e}\| \;\lesssim\; \Big(m_1(\underline{e},\mathcal{T}) + m_1(\underline{v}_\varepsilon,\mathcal{T})\Big)(\eta+\zeta). \tag{44}$$

Proof: Follows directly from Lemmas 6.5 and 6.6. ∎

6.3.3 Error in the velocity - Nonconforming case

Lemma 6.8 (Error orthogonality) *In the 2D case, for any vector valued function $\underline{s}^I \in [\mathrm{Im}(\mathrm{I}_{\mathrm{Cl}})]^2$, one has the error orthogonality*

$$\int_\Omega \nabla_{\mathcal{T}}\,\underline{e} \,:\, \underline{\mathrm{curl}}\,\underline{s}^I = 0. \tag{45}$$

Similarly, in the 3D case one has for any matrix function $\underline{\underline{s}}^I \in [\mathrm{Im}(\mathrm{I}_{\mathrm{Cl}})]^{3\times 3}$

$$\int_\Omega \nabla_{\mathcal{T}}\,\underline{e} \,:\, \underline{\underline{\mathrm{curl}}}\,\underline{\underline{s}}^I = -\sum_{E\in\mathcal{E}_\square}\int_E [\![\underline{u}_h]\!]_E \cdot (\underline{\underline{\mathrm{curl}}}\,\underline{\underline{s}}^I\,\underline{n}_E), \tag{46}$$

i.e. the sum is only over the rectangular faces $E \in \mathcal{E}_\square$.

Proof: In the 2D case, by means of (5) one concludes

$$
\begin{aligned}
\int_\Omega \nabla_{\mathcal{T}}\,\underline{e} \,:\, \underline{\mathrm{curl}}\,\underline{s}^I \;&=\; \int_\Omega \nabla\underline{u} \,:\, \underline{\mathrm{curl}}\,\underline{s}^I \;-\; \sum_{T\in\mathcal{T}}\int_T \nabla\underline{u}_h \,:\, \underline{\mathrm{curl}}\,\underline{s}^I \\
&\overset{(5)}{=}\; -\int_{\partial\Omega}\underline{u}\cdot(\nabla\underline{s}^I\,\underline{t}) \;+\; \sum_{T\in\mathcal{T}}\int_{\partial T}\underline{u}_h\cdot(\nabla\underline{s}^I\,\underline{t}) \\
&=\; -\sum_{E\in\mathcal{E}}\int_E [\![\underline{u}_h]\!]_E\cdot(\nabla\underline{s}^I\,\underline{t}_E) \;=\; 0
\end{aligned}
$$

since $\underline{u} = \underline{0}$ on $\partial\Omega$, and due to the assumption (CR) and the fact that $(\nabla\underline{s}^I\,\underline{t}_E)|_E$ is always constant.

In 3D one employs (6) instead of (5) to conclude

$$\int_\Omega \nabla_{\mathcal{T}}\,\underline{e} \,:\, \underline{\underline{\mathrm{curl}}}\,\underline{\underline{s}}^I = -\sum_{E\in\mathcal{E}}\int_E [\![\underline{u}_h]\!]_E \cdot (\underline{\underline{\mathrm{curl}}}\,\underline{\underline{s}}^I\,\underline{n}_E).$$

There we utilize that $\underline{\underline{\mathrm{curl}}}\,\underline{\underline{s}}^I\underline{n}_E$ is continuous across a face E. This holds since $(\underline{\underline{\mathrm{curl}}}\,\underline{\underline{s}}^I\underline{n}_E)|_E$ contains only tangential derivatives (on a face E).

Furthermore, for a triangular face $E_\triangle$ of a triangulation a closer inspection reveals that $\underline{\underline{\mathrm{curl}}}\,\underline{\underline{s}}^I|_{E_\triangle}$ is constant for $\underline{\underline{s}}^I \in [\mathrm{Im}(\mathrm{I}_{\mathrm{Cl}})]^{3\times 3}$. Due to the Crouzeix-Raviart property (CR),

the corresponding contribution to the sum vanishes, and we end up with the sum over the rectangular faces alone.

As a side effect, (46) vanishes for triangulations consisting solely of tetrahedra. ∎

Next we will estimate the remaining non-vanishing terms of (46) that arise from rectangular faces.

Lemma 6.9 *In the 3D case for any matrix function $\underline{\underline{s}}^I \in [\mathrm{Im}(\mathrm{I_{Cl}})]^{3\times 3}$ and any rectangular face $E \in \mathcal{E}_\square$ we have*

$$\left| \int_E [\![\underline{u}_h]\!]_E \cdot (\underline{\underline{\mathrm{curl}}}\ \underline{\underline{s}}^I\ \underline{n}_E) \right| \lesssim \|[\![\underline{u}_h]\!]_E\|_E\ \varrho(E)^{-1}\|\underline{\underline{s}}^I - \mathcal{M}_E\underline{\underline{s}}^I\|_E, \tag{47}$$

where $\mathcal{M}_E$ is the face mean operator introduced in Lemma 4.4.

Proof: By Cauchy-Schwarz's inequality we have

$$\left| \int_E [\![\underline{u}_h]\!]_E \cdot (\underline{\underline{\mathrm{curl}}}\ \underline{\underline{s}}^I\ \underline{n}_E) \right| \leq \|[\![\underline{u}_h]\!]_E\|_E\ \|\underline{\underline{\mathrm{curl}}}\ \underline{\underline{s}}^I\ \underline{n}_E\|_E.$$

The second factor of this right-hand side is estimated using a scaling argument. Note in particular that $\underline{\underline{\mathrm{curl}}}\ \underline{\underline{s}}^I\ \underline{n}_E$ involves only tangential derivatives of $\underline{\underline{s}}^I$, and that it is rotationally invariant. ∎

Lemma 6.10 (Error in the velocity - Nonconforming case.) *In the 2D case, there exist functions $\underline{r} \in [H_0^1(\Omega)]^2, \underline{s} \in [H^1(\Omega)]^2$ both depending on $\underline{e} = \underline{u} - \underline{u}_h$ such that the error in the velocity is bounded by*

$$\|\nabla_{\mathcal{T}}\,\underline{e}\| \lesssim \Big(m_1(\underline{r}, \mathcal{T}) + m_1(\underline{s}, \mathcal{T})\Big)(\eta + \zeta). \tag{48}$$

In the 3D case the vector function $\underline{s}$ is replaced by a matrix function $\underline{\underline{s}} \in [H^1(\Omega)]^{3\times 3}$.

Proof: Start with the 2D case. Following [DDP95, Lemma 3.2], there exists a Helmholtz like decomposition of the error as

$$\nabla_{\mathcal{T}}\,\underline{e}\ =\ \nabla\underline{r} - q\mathrm{I} + \underline{\underline{\mathrm{curl}}}\ \underline{s},$$

with $\underline{r} = \underline{r}(\underline{e}) \in [H_0^1(\Omega)]^2, q = q(\underline{e}) \in L_0^2(\Omega), \underline{s} = \underline{s}(\underline{e}) \in [H^1(\Omega)]^2$, and the additional properties

$$\|\nabla\underline{r}\| + \|\nabla\underline{s}\| + \|q\| \lesssim \|\nabla_{\mathcal{T}}\,\underline{e}\|, \tag{49}$$
$$\mathrm{div}\,\underline{r} = 0.$$

Using $\mathrm{div}\,\underline{r} = 0$ and $\mathrm{div}\,\underline{u} = 0$ one obtains

$$\begin{aligned}
\|\nabla_{\mathcal{T}}\,\underline{e}\|^2 &= \int_\Omega \nabla_{\mathcal{T}}\,\underline{e} : (\nabla\underline{r} - q\mathrm{I} + \underline{\underline{\mathrm{curl}}}\ \underline{s}) \\
&= \int_\Omega (\nabla_{\mathcal{T}}\,\underline{e} : \nabla\underline{r} - \varepsilon\mathrm{div}\,\underline{r}) + \int_\Omega \mathrm{div}_{\mathcal{T}}\underline{u}_h\, q + \int_\Omega \nabla_{\mathcal{T}}\,\underline{e} : \underline{\underline{\mathrm{curl}}}\ \underline{s}.
\end{aligned}$$

Next, we take the Clément interpolants $I_{Cl}^0\underline{r}$ and $I_{Cl}\underline{s}$ (note the different interpolation operators to reflect the different boundary data). Apply the orthogonality relations (10) and (45) and integrate by parts to reformulate

$$\|\nabla_{\mathcal{T}}\,\underline{e}\,\|^2 \overset{(10),(45)}{=} \int_{\Omega}(\nabla_{\mathcal{T}}\,\underline{e}\,:\nabla(\underline{r}-I_{Cl}^0\underline{r})-\varepsilon\mathrm{div}\,(\underline{r}-I_{Cl}^0\underline{r}))+\int_{\Omega}\nabla_{\mathcal{T}}\,\underline{e}\,:\underline{\underline{\mathrm{curl}}}\,(\underline{s}-I_{Cl}\underline{s})$$

$$+\int_{\Omega}\mathrm{div}_{\mathcal{T}}\underline{u}_h\,q$$

$$\overset{(3),(4),(5)}{=} \int_{\Omega}(-\Delta\underline{u}+\nabla p)\cdot(\underline{r}-I_{Cl}^0\underline{r})+\int_{\partial\Omega}(\nabla\underline{u}-p\mathrm{I})\underline{n}\cdot(\underline{r}-I_{Cl}^0\underline{r})$$

$$+\int_{\partial\Omega}\nabla\underline{u}\,\underline{t}\cdot(\underline{s}-I_{Cl}\underline{s})$$

$$-\sum_{T\in\mathcal{T}}\Big\{\int_T(-\Delta\underline{u}_h+\nabla p_h)\cdot(\underline{r}-I_{Cl}^0\underline{r})+\int_{\partial T}(\nabla\underline{u}_h-p_h\mathrm{I})\underline{n}\cdot(\underline{r}-I_{Cl}^0\underline{r})$$

$$+\int_{\partial T}\nabla\underline{u}_h\underline{t}\cdot(\underline{s}-I_{Cl}\underline{s})\Big\}$$

$$+\int_{\Omega}\mathrm{div}_{\mathcal{T}}\underline{u}_h\,q$$

$$= \sum_{T\in\mathcal{T}}\int_T\underline{R}_T\cdot(\underline{r}-I_{Cl}^0\underline{r})\ +\ \sum_{E\in\mathcal{E}}\int_E\underline{J}_{E,n}\cdot(\underline{r}-I_{Cl}^0\underline{r})$$

$$+\sum_{E\in\mathcal{E}}\int_E\underline{J}_{E,t}\cdot(\underline{s}-I_{Cl}\underline{s})\ +\ \int_{\Omega}\mathrm{div}_{\mathcal{T}}\underline{u}_h\,q.$$

The interpolation estimates (20), (21), (22) of Lemma 4.4 then yield

$$\|\nabla_{\mathcal{T}}\,\underline{e}\,\|^2 \lesssim \Big(\sum_{T\in\mathcal{T}}h_{min,T}^2\|\underline{R}_T\|_T^2\Big)^{1/2}m_1(\underline{r},\mathcal{T})\,\|\nabla\underline{r}\|$$

$$+\Big(\sum_{E\in\mathcal{E}}h_{min,T}^2 h_E^{-1}\|\underline{J}_{E,n}\|_E^2\Big)^{1/2}m_1(\underline{r},\mathcal{T})\,\|\nabla\underline{r}\|$$

$$+\Big(\sum_{E\in\mathcal{E}}h_{min,T}^2 h_E^{-1}\|\underline{J}_{E,t}\|_E^2\Big)^{1/2}m_1(\underline{s},\mathcal{T})\,\|\nabla\underline{s}\|$$

$$+\|\mathrm{div}_{\mathcal{T}}\underline{u}_h\|\,\|q\|$$

$$\le (\eta+\zeta)\Big(m_1(\underline{r},\mathcal{T})\,\|\nabla\underline{r}\|+m_1(\underline{s},\mathcal{T})\,\|\nabla\underline{s}\|+\|q\|\Big).$$

Finally apply the *a priori* bound (49) to finish the proof.

In the 3D case, the decomposition of $\nabla_{\mathcal{T}}\,\underline{e}$ changes and contains a *matrix* function $\underline{s}\in[H^1(\Omega)]^{3\times3}$ instead (see Theorem I.3.4 in [GR86]). Consequently the partial integration of the $\underline{\underline{\mathrm{curl}}}$ terms is modified which eventually leads to the adapted definition of the tangential jump $\underline{J}_{E,t}$. Furthermore in the above expansion of $\|\nabla_{\mathcal{T}}\,\underline{e}\,\|^2$ the additional term

$\int_\Omega \nabla_{\mathcal{T}} \underline{e} : \underline{\text{curl}}\, \mathrm{I}_{\mathrm{Cl}}\underline{s}$ is no longer zero. Using the identity (46) and the estimate (47) from Lemma 6.9 we get successively

$$\left| \int_\Omega \nabla_{\mathcal{T}} \underline{e} : \underline{\text{curl}}\, \mathrm{I}_{\mathrm{Cl}}\underline{s} \right| \lesssim \sum_{E \in \mathcal{E}_\square} \|[\![\underline{u}_h]\!]_E\|_E \varrho(E)^{-1} \|\mathrm{I}_{\mathrm{Cl}}\underline{s} - \mathcal{M}_E \mathrm{I}_{\mathrm{Cl}}\underline{s}\|_E$$

$$\leq \left(\sum_{E \in \mathcal{E}_\square} h_{min,E}^2 h_E^{-1} \varrho(E)^{-2} \|[\![\underline{u}_h]\!]_E\|_E^2 \right)^{1/2} \left(\sum_{E \in \mathcal{E}_\square} h_{min,E}^{-2} h_E \|\mathrm{I}_{\mathrm{Cl}}\underline{s} - \mathcal{M}_E \mathrm{I}_{\mathrm{Cl}}\underline{s}\|_E \right)^{1/2}.$$

The estimate (23) of Lemma 4.4 and the definition of the residual error estimator finally lead to

$$\left| \int_\Omega \nabla_{\mathcal{T}} \underline{e} : \underline{\text{curl}}\, \mathrm{I}_{\mathrm{Cl}}\underline{s} \right| \lesssim \eta\, m_1(\underline{s}, \mathcal{T})\, \|\nabla \underline{s}\|.$$

∎

The inequalities of the previous lemmas provide the main upper error bound for non-conforming discretizations.

Theorem 6.11 (Upper error bound - Nonconforming case.) *Let $\underline{v}_\varepsilon$ and $\underline{r}, \underline{s}$ be the functions from Lemma 6.5 and 6.10. Then the error is bounded globally from above by*

$$\|\varepsilon\| + \|\nabla_{\mathcal{T}} \underline{e}\| \lesssim \Big(m_1(\underline{r}, \mathcal{T}) + m_1(\underline{s}, \mathcal{T}) + m_1(\underline{v}_\varepsilon, \mathcal{T}) \Big)(\eta + \zeta). \tag{50}$$

In the 3D case the vector function $\underline{s}$ is replaced by a matrix function $\underline{\underline{s}} \in [H^1(\Omega)]^{3 \times 3}$.

Proof: Follows directly from the aforementioned lemmas. ∎

Remark 6.12 (Rectangular jump) *We may see that the rectangular jump only appears in the estimate of the left-hand side of (46) via Lemmas 6.9 and 4.4. As an alternative we may impose a stronger assumption than (CR) on rectangular faces, namely*

$$\int_E [\![\underline{u}_h]\!]_E q = 0, \qquad \forall \underline{u}_h \in V_{\text{veloc}}, q \in \mathbb{P}^1(E), E \in \mathcal{E}_\square. \tag{CR'}$$

This last assumption leads to the orthogonality relation (45) and then allows to avoid the use of the rectangular jump. But the construction of element pairs fulfilling (CR) on triangular faces and (CR') on rectangular faces and being stable seems to be difficult and unrealistic.

Remark 6.13 (Alignment measure) *The upper error bounds (e.g. (44) and (50)) contain several alignment measures $m_1(\cdot, \mathcal{T})$. This is in contrast to estimators for isotropic meshes: For anisotropic discretizations, all known estimators are (explicitly or implicitly) based on an anisotropic mesh that is suitably aligned with the anisotropic function.*

Compared with the isotropic estimators, our upper error bounds are special in the sense that the alignment measure cannot be evaluated explicitly. However, this should not be

considered too much as a disadvantage. For example, the alignment measure $m_1(\underline{e}, \mathcal{T})$ for the error $\underline{e} = \underline{u} - \underline{u}_h$ is of size $\mathcal{O}(1)$ for sufficiently good meshes, cf. [Kun00, Kun01, Kun02]. We expect a similar behaviour for the other alignment measures. This confidence is strengthened by the numerical experiments below.

In practical computations one may simply use the error estimator without considering the alignment measures. For adaptive algorithms this is well justified since the lower error bound holds unconditionally (with the exception of nonconforming 3D triangulations made of pentahedra or hexahedra), i.e. the estimator is efficient.

6.4 Application to isotropic discretizations

On *isotropic* discretizations, our analysis covers the case of stable pairs like the Mini element, the Hood-Taylor element, or nonconforming elements of Crouzeix-Raviart type, see Table 1 below. Then our analysis and the conclusions hold with $h_{min,T} \sim h_E \sim h_T$ for $E \subset \partial T$ and the alignment measure $m_1(\cdot, \mathcal{T}) \sim 1$. In other words, the above results may be rephrased as follows: the residual error estimator is here given by

$$\eta_T^2 := h_T^2 \|\underline{r}_T\|_T^2 + \|\mathrm{div}\, \underline{u}_h\|_T^2 + h_T \sum_{E \subset \partial T} \left(\|\underline{J}_{E,n}\|_E^2 + \|\underline{J}_{E,t}\|_E^2 \right),$$

while the approximation term becomes

$$\zeta_T^2 := h_T^2 \sum_{T' \subset \omega_T} \|\underline{r}_{T'} - \underline{R}_{T'}\|_{T'}^2,$$

where we recall that h_T is the diameter of T. With these definitions, the lower error bound (36) of Theorem 6.2 holds for any isotropic elements T. On the other hand the upper bounds (44) and (50) reduce to

$$\|\varepsilon\| + \|\nabla_\mathcal{T}\, \underline{e}\| \lesssim \eta + \zeta.$$

Table 1 provides a list of stable elements covered by our analysis. The last column gives alternative references where some equivalences between the error and the *residual* error estimator have been proved (other kinds of estimators are omitted).

7 Numerical experiments

The following experiments will underline and confirm our theoretical predictions. This example consists in solving the two dimensional Stokes problem (1) on the unit square $\Omega = (0,1)^2$. Here, we use the Crouzeix-Raviart element II (see Section 5.2), on an anisotropic Shishkin type mesh composed of rectangles. This mesh is the tensor product of a 1D Shishkin type mesh and a uniform mesh, both with n subintervals. With $\tau \in (0,1)$ being a transition point parameter, the coordinates (x_i, y_j) of the nodes of the rectangles are defined by

$$dx_1 := 2\tau/n, \quad dx_2 := 2(1-\tau)/n, \quad dy = 1/n,$$

Discretization	Element	Velocity / Pressure spaces	Name	Ref. on residual error estimators
2D/conf.	Triangle	$[P_1 + \text{el. bubble}]^2 \ / \ P_{1c}$	Mini element	[Ver89]
2D/conf.	Triangle	$[P_2]^2 \ / \ P_{1c}$	Hood-Taylor	[Ver89](claimed) [Bur01](up. bound)
2D/conf.	Triangle	$[P_1]^2 + \text{face bubbles} \cdot n_E \ / \ P_0$	BFR	[CF01]
2D/conf.	Rectangle	$[Q_1]^2 + \text{face bubbles} \cdot n_E \ / \ P_0$	BFR	[CF01]
2D/conf.	Triangle	$[P_l \oplus \lambda_1 \lambda_2 \lambda_3 \tilde{P}_{l-2}]^2 \ / \ P_{l-1} \quad l \geq 2$	conforming CR	[CF01]
2D/conf	Rectangle	$[Q_l]^2 / P_{l-1}, l \geq 2$		[CF01]
2D/non conf.	Triangle	$[P_1]^2 / P_0$	CR	[DDP95], [CF01]
2D/non conf.	Rectangle	$[P_2]^2 / P_0$	Section 5.3	
2D/non conf.	Triangle	$[P_2]^2 / P_1$	Fortin-Soulie	[DDP95]
3D/conf.	Tetra	$[P_1 + \text{el. bubble}]^3 \ / \ P_{1c}$	Mini element	
3D/conf.	Tetra	$[P_2]^3 \ / \ P_{1c}$	Hood-Taylor	[Bur01](up. bound)
3D/conf.	Tetra	$[P_1]^3 + \text{face bubbles} \cdot n_E \ / \ P_0$	BFR	
3D/conf	Tetra	$[P_2 \oplus \lambda_1 \lambda_2 \lambda_3 \lambda_4 P_0]^3 +\text{face bubbles} \cdot n_E \ / \ P_1$	High order BFR	
3D/non conf.	Tetra	$[P_1]^3 / P_0$	CR	
3D/non conf.	Penta	$[\mathbb{P}^2]^3 \ / \ P_0$	Section 5.4	
3D/non conf.	Hexa	$[\mathbb{P}^2 + xyz]^3 \ / \ P_0$	Section 5.5	

Table 1: Stable isotropic elements covered

$$\begin{cases} x_i & := & i \, dx_1 & (0 \leq i \leq n/2), \\ x_i & := & \tau + (i - n/2) \, dx_2 & (n/2 + 1 \leq i \leq n), \\ y_j & := & j \, dy & (0 \leq j \leq n). \end{cases}$$

The discrete problem (9) is solved with the Uzawa algorithm. The number of degrees of freedom is equal to $n(3n + 2)$ for each component of the velocity, and equals n^2 for the pressure. The total number of degrees of freedom (DoF) is then equal to $n(7n + 4)$.

The tests are performed with the following prescribed exact solution $(\underline{u}, p)$:

$$\begin{cases} \Phi & = & x^2(1 - x)^2 y^2 (1 - y)^2 e^{-x/\sqrt{\varepsilon}}, \\ \underline{u} & = & \underline{\text{curl}} \ \Phi, \\ p & = & e^{-x/\sqrt{\varepsilon}}. \end{cases}$$

This allows to have in particular $\text{div} \, \underline{u} \ = \ 0$ and $\underline{u}_{|\Gamma} = 0$. Note that $\underline{u}$ and p present
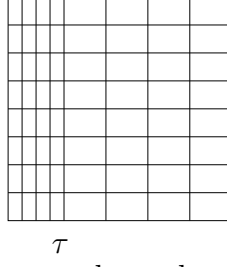
Figure 1: Shishkin type mesh on the unit square with $n = 8$.

an exponential boundary layer of width $\mathcal{O}(\sqrt{\varepsilon})$ along the line $x = 0$. The transition parameter τ involved in the construction of the Shishkin-type mesh is defined by $\tau := \min\{1/2, 2\sqrt{\varepsilon}|\ln\sqrt{\varepsilon}|\}$, i.e. it is roughly twice the boundary layer width. The maximal aspect ratio in the mesh is equal to $1/(2\tau)$.

To begin with, let us check that the numerical solution $(\underline{u}_h, p_h)$ converges towards the exact one. To this end we plot the curves

- $||\nabla_{\mathcal{T}}(\underline{u} - \underline{u}_h)||_\Omega$ as a function of DoF (see Figure 2 left),

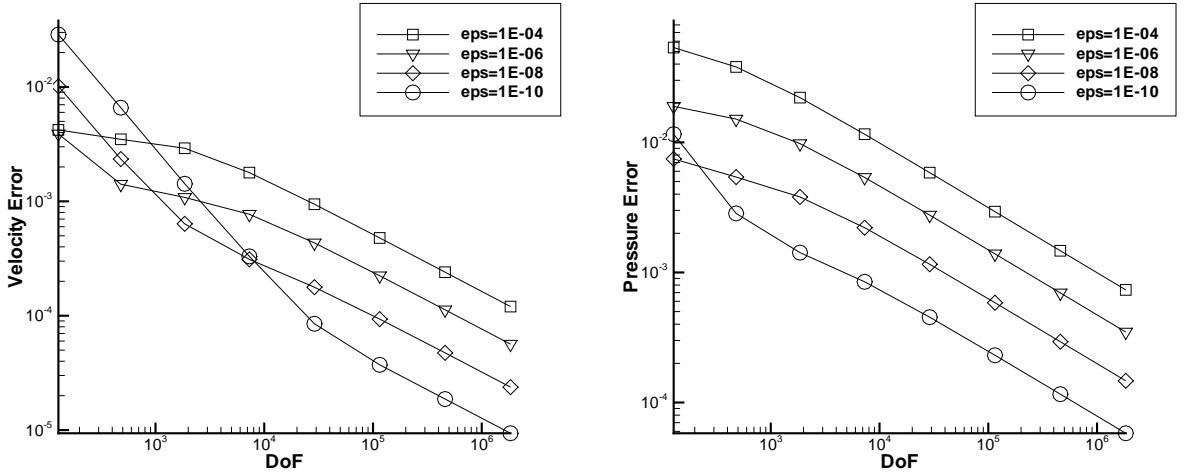- $||p - p_h||_\Omega$ as a function of DoF (see Figure 2 right).

Figure 2: $||\nabla_h(\underline{u} - \underline{u}_h)||_\Omega$ (left) and $||p - p_h||_\Omega$ (right) in dependence of DoF.

As we can see, the convergence rates for the velocity and for the pressure are of order 0.5, as theoretically expected. This shows the good convergence of $(\underline{u}_h, p_h)$ towards $(\underline{u}, p)$.

Now we investigate the main theoretical results which are the upper and the lower error bounds. In order to present the underlying inequalities (36) and (50) appropriately, we reformulate them by defining the ratios of left-hand side and right-hand side, respectively:

- $q_{\mathrm{up}} = \dfrac{||\nabla_{\mathcal{T}}\,(\underline{u}\,-\,\underline{u}_h)||_\Omega + ||p - p_h||_\Omega}{\eta + \zeta}$ as a function of $DoF,$

- $q_{\mathrm{low}} = \max\limits_{T \in \mathcal{T}} \dfrac{\eta_T}{||\nabla_{\mathcal{T}}\,(\underline{u}\,-\,\underline{u}_h)||_{\omega_T} + ||p - p_h||_{\omega_T} + \zeta_T}$ as a function of $DoF.$

The second ratio is related to the local lower error bound and measures the *efficiency* of the estimator. According to Theorem 6.2, q_{low} has to be bounded from above. This can be observed indeed in the right part of Figure 3. Hence the estimator is *efficient*. Note that the values of q_{low} are much alike the ones for other problem classes, cf. [Kun00, Kun01].

The first ratio q_{up} is frequently referred to as *effectivity index*. It measures the *reliability* of the estimator and is related to the global upper error bound. In order to investigate this error bound, recall first that the alignment measures $m_1(\cdot, \mathcal{T})$ are expected to be of moderate size since we employ well adapted meshes (cf. Theorem 6.11). Hence the corresponding ratio q_{up} should be bounded from above which is confirmed by the experiment (left part of Figure 3). As soon as a reasonable resolution of the layer is achieved, the quality of the upper error bound is independent of ε. Thus the estimator is *reliable*. Again the values of q_{up} resemble the ones for other problem classes, cf. above.
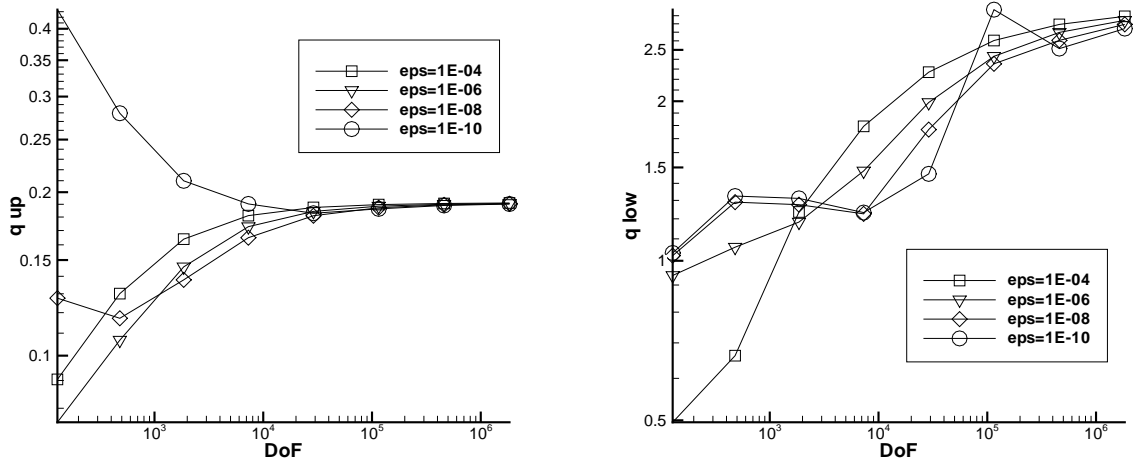

Figure 3: q_{up} (left) and q_{low} (right) in dependence of DoF.

8   Summary

We have proposed and analysed *a posteriori* residual type error estimators for the Stokes problem on *anisotropic* meshes. Our investigations cover conforming and nonconforming discretizations, 2D and 3D domains as well as different kinds of elements. Much effort has been taken to impose as few assumptions as possible. For nonconforming discretizations, the main demand consists in Crouzeix-Raviart type elements.

The upper error bounds of Theorems 6.7 and 6.11 form two of the main results. In order to obtain sharp bounds, the anisotropic mesh has to be properly aligned, as it is the case with all known anisotropic (*a posteriori*) estimators. Here, this alignment enters explicitly via a so-called alignment measure. In contrast to previous work (e.g. [Kun00, Kun01]), this mesh alignment is not with respect to the error $\underline{e} = \underline{u} - \underline{u}_h$ but also with respect to other functions (cf. Theorems 6.7 and 6.11). As numerical tests confirm, this is only a minor disadvantage.

Another main result is given by the local lower error bound of Theorem 6.2 which could be proven for almost all cases. Only nonconforming 3D discretizations consisting of pentahedra or hexahedra are exceptional where only a (weaker) global lower bound is obtained.

For *isotropic* discretizations, much of the analysis simplifies. The main results are presented in Section 6.4. The investigations seem to be novel for most 3D elements.

Numerical results accompany and confirm the theoretical predictions.

References

[AN]   Th. Apel and S. Nicaise. On the inf-sup condition for the Bernardi–Fortin–Raugel element on anisotropic meshes. Technical report. To appear.

[ANS01a] Th. Apel, S. Nicaise, and J. Schöberl. Crouzeix-Raviart type finite elements on anisotropic meshes. *Numer. Math.*, 89:193–223, 2001.

[ANS01b] Th. Apel, S. Nicaise, and J. Schöberl. A non-conforming finite element method with anisotropic mesh grading for the Stokes problem in domains with edges. *IMA J. Numer. Anal.*, 21:843–856, 2001.

[AO97]   M. Ainsworth and J.T. Oden. A posteriori error estimators for the Stokes and Oseen equations. *SIAM J. Num. Anal.*, 34(1):228–245, 1997.

[Ape99]   Th. Apel. *Anisotropic finite elements: Local estimates and applications*. Advances in Numerical Mathematics. Teubner, Stuttgart, 1999.

[Ban98]   R. E. Bank. A simple analysis of some a posteriori error estimates. *Appl. Numer. Math.*, 26(1-2):153–164, 1998.

[Bec00]   R. Becker. An optimal control approach to a posteriori error estimation for finite element discretizations of the navier-stokes equations. *East-West J. Numer. Math.*, 8(4):257–274, 2000.

[Bur01]   P. Burda. A posteriori error estimates for the Stokes flow in 2D and 3D domains. In P. Neittaanmkiet al., editor, *Finite element methods. Three-dimensional problems*, volume 15 of *GAKUTO Int. Ser., Math. Sci. Appl*, pages 34–44. Gakkotosho, 2001.

[BW90]   R. E. Bank and B. D. Welfert. A posteriori error estimates for the Stokes
          equations: a comparison. *Comput. Methods Appl. Mech. Engrg.*, 82:323–340,
          1990.

[CF01]   C. Carstensen and S. Funken. A posteriori error control in low-order finite ele-
          ment discretisations of incompressible stationary flow problems. *Math. Comp.*,
          70(236):1353–1381, 2001.

[Cia78]   P. G. Ciarlet. *The finite element method for elliptic problems.* North-Holland,
          Amsterdam, 1978.

[CR73]   M. Crouzeix and P. A. Raviart. Conforming and non-conforming finite elements
          for solving the stationary Stokes equations. *R.A.I.R.O. Anal. Numér.*, 7:33–76,
          1973.

[DDP95]   E. Dari, R. Durán, and C. Padra. Error estimators for nonconforming finite
          element approximations of the stokes problem. *Math. Comput.*, 64(211):1017–
          1033, 1995.

[DGP99]   M. Dobrowolski, S. Gräf, and C. Pflaum. On a posteriori error estimators
          in the finite element method on anisotropic meshes. *Electronic Transactions
          Num. Anal.*, 8:36–45, 1999.

[FPZ01]   L. Formaggia, S. Perotto, and P. Zunino. An anisotropic a-posteriori error
          estimate for a convection-diffusion problem. *Comput. Vis. Sci.*, 4(2):99–104,
          2001.

[GR86]   V. Girault and P.-A. Raviart. *Finite element methods for Navier-Stokes equa-
          tions, Theory and algorithms*, volume 5 of *Springer Series in Computational
          Mathematics.* Springer, Berlin, 1986.

[JL00]   J. Jou and J.-L. Liu. An a posteriori finite element error analysis for the stokes
          equations. *J. Comput. Appl. Math.*, 14(2):333–343, 2000.

[Joh98]   V. John. A posteriori L^2-error estimates for the nonconforming P_1/P_0-finite ele-
          ment discretization of the Stokes equations. *J. Comput. Appl. Math.*, 96(2):99–
          116, 1998.

[KS00]   D. Kay and D. Silvester. A posteriori error estimation for stabilized mixed
          approximations of the Stokes equations. *SIAM J. Sci. Comput.*, 21(4):1321–
          1336, 2000.

[Kun99]   G. Kunert. *A posteriori error estimation for anisotropic tetrahedral and trian-
          gular finite element meshes.* Logos Verlag, Berlin, 1999. Also PhD thesis, TU
          Chemnitz, http://archiv.tu-chemnitz.de/pub/1999/0012/index.html.

[Kun00]   G. Kunert. An a posteriori residual error estimator for the finite element method on anisotropic tetrahedral meshes. *Numer. Math.*, 86(3):471–490, 2000. DOI 10.1007/s002110000170.

[Kun01]   G. Kunert. Robust a posteriori error estimation for a singularly perturbed reaction–diffusion equation on anisotropic tetrahedral meshes. *Adv. Comp. Math.*, 15(1–4):237–259, 2001.

[Kun02]   G. Kunert. Towards anisotropic mesh construction and error estimation in the finite element method. *Numer. Meth. PDE*, 18(6):625–648, 2002.

[Ran01]   M. Randrianarivony. Strengthened Cauchy inequality in anisotropic meshes and application to an a-posteriori error estimator for the Stokes problem. Preprint SFB393/01–23, TU Chemnitz, 2001.

[Sie96]   K. G. Siebert. An a posteriori error estimator for anisotropic refinement. *Numer. Math.*, 73(3):373–398, 1996.

[Ver89]   R. Verfürth. A posteriori error estimators for the Stokes equation. *Numer. Math.*, 55:309–325, 1989.

[Ver91]   R. Verfürth. A posteriori error estimators for the Stokes equation ii : nonconforming discretizations. *Numer. Math.*, 60:235–249, 1991.

[Ver96]   R. Verfürth. *A review of a posteriori error estimation and adaptive mesh–refinement techniques.* Wiley-Teubner, Chichester; Stuttgart, 1996.

Gerd Kunert   Emmanuel Creusé, Serge Nicaise
TU Chemnitz   Université de Valenciennes et du Hainaut Cambrésis
Fakultät für Mathematik   MACS
09107 Chemnitz   59313 Valenciennes Cedex 9
Germany   France

gerd.kunert@mathematik.tu-chemnitz.de
http://www.tu-chemnitz.de/∼gku
http://www.tu-chemnitz.de/sfb393/

Emmanuel.Creuse@univ-valenciennes.fr
http://www.univ-valenciennes.fr/macs/Emmanuel.Creuse/Page_accueil.html

snicaise@univ-valenciennes.fr
http://www.univ-valenciennes.fr/macs/Serge.Nicaise/accueil.htm